



HAL
open science

An analytical model for azimuthal thermo-acoustic modes in annular chamber fed by an annular plenum

Michael Bauerheim, Jean-François Parmentier, Pablo Salas, Franck Nicoud,
Thierry Poinsot

► **To cite this version:**

Michael Bauerheim, Jean-François Parmentier, Pablo Salas, Franck Nicoud, Thierry Poinsot. An analytical model for azimuthal thermo-acoustic modes in annular chamber fed by an annular plenum. *Combustion and Flame*, 2014, 161 (5), pp.1374 - 1389. 10.1016/j.combustflame.2013.11.014 . hal-00969565

HAL Id: hal-00969565

<https://hal.science/hal-00969565v1>

Submitted on 2 Apr 2014

HAL is a multi-disciplinary open access archive for the deposit and dissemination of scientific research documents, whether they are published or not. The documents may come from teaching and research institutions in France or abroad, or from public or private research centers.

L'archive ouverte pluridisciplinaire **HAL**, est destinée au dépôt et à la diffusion de documents scientifiques de niveau recherche, publiés ou non, émanant des établissements d'enseignement et de recherche français ou étrangers, des laboratoires publics ou privés.

An analytical model for azimuthal thermo-acoustic modes in annular chamber fed by an annular plenum

M. Bauerheim^a, J.-F. Parmentier^a, P. Salas^b, F. Nicoud^c, T. Poinsot^d

^a*CERFACS, CFD team, 42 Av Coriolis, 31057 Toulouse, France*

^b*INRIA Bordeaux - Sud Ouest, HiePACS Project, joint INRIA-CERFACS lab. on High Performance Computing*

^c*Université Montpellier 2. I3M.UMR CNRS 5149*

^d*IMF Toulouse, INP de Toulouse and CNRS, 31400 Toulouse, France*

Abstract

This study describes an analytical method to compute azimuthal modes due to flame/acoustics coupling in annular combustors. It is based on a quasi-one-dimensional zero-Mach number formulation where N burners are connected to an upstream annular plenum and a downstream chamber. Flames are supposed to be compact and are modeled using identical Flame Transfer Function for all burners, characterized by an amplitude and a phase shift. Manipulation of the corresponding acoustic equations leads to a simple methodology called ANR (Annular Network Reduction). It allows to retain only the useful information related to the azimuthal modes of the annular cavities. It yields a simple dispersion relation which can be solved numerically and allows to construct coupling factors between the different cavities of the combustor. A fully analytical resolution can be performed in specific situations where coupling factors are small (weak coupling). A bifurcation appears at high coupling factors leading to a frequency lock-in of the two annular cavities (strong coupling). This tool is applied to an academic case where four burners connect an annular plenum to a chamber. For this configuration, analytical results are compared to a full three-dimensional Helmholtz solver to validate the analytical model in both weak and strong coupling regimes. Results show that this simple analytical tool allows to predict modes in annular combustors and investigate strategies to control them.

Keywords: azimuthal modes, analytical, combustion instabilities, coupling

Nomenclature

$\alpha = z_{f,i}/L_i$ Normalized abscissa for the flame location in the burners

$\beta = \frac{c^0 L_p}{c_u^0 L_c}$ Tuning parameter

ϵ_p and ϵ_c Wavenumber perturbation in the plenum and chamber

$\Gamma_{i,k}$ k^{th} coupling parameter of the i^{th} sector

$\mathbb{F} = \frac{\rho^0 c^0}{\rho_u^0 c_u^0} (1 + n_i e^{j\omega\tau_i})$ Flame parameter

ω Angular frequency

ρ_u^0 and ρ^0 Mean density in the unburnt and burnt gases

τ_i Time-delay of the FTF of the i^{th} flame

$\tau_p^0 = \frac{2c_u^0}{pL_p}$ and $\tau_c^0 = \frac{2c^0}{pL_c}$ Period of the unperturbed p^{th} azimuthal mode of the plenum and chamber

θ Angle in the annular cavities

c_u^0 and c^0 Mean sound speed in the unburnt and burnt gases

k_u and k Wavenumber in the unburnt and burnt gases

$L_c = \pi R_c$ and $L_p = \pi R_p$ Half perimeter of the chamber or plenum

L_i Length of the i^{th} burner

N Number of burners

n_i Interaction index of the FTF of the i^{th} flame

p Order of the azimuthal mode

p' Pressure fluctuations

R_c and R_p Radii of the annular chamber or plenum

S_c , S_p and S_i Cross-section of the chamber, plenum and i^{th} burner

u' Azimuthal velocity fluctuations (along x)

- w' Axial velocity fluctuations (along z)
- x Azimuthal abscissa in the chamber or plenum corresponding to $x_c = R_c\theta$ or $x_p = R_p\theta$
- z Longitudinal abscissa in the burners
- ANR Annular Network Reduction
- ATACAMAC Analytical Tool to Analyze and Control Azimuthal Modes in Annular Combustors
- BC Burners+Chamber configuration (Fig.1 left)
- BCp Burner+Chamber mode of order p (the annular plenum is perfectly decoupled from the system)
- FDCp Full Decoupled Chamber mode of order p
- FDPp Fully Decoupled Plenum mode of order p
- FTF Flame Transfer Function
- LES Large Eddy Simulation
- PBC Plenum+Burners+Chamber configuration (Fig.1 right)
- PBp Plenum+Burner mode of order p (the annular chamber is perfectly decoupled from the system)
- SCp Strongly Coupled mode of order p
- WCCp Weakly Coupled Chamber mode of order p
- WCPp Weakly Coupled Plenum mode of order p

1. Introduction

Describing the unstable acoustic modes which appear in annular gas turbine combustion chambers and finding methods to control them is the topic of multiple present research activities [1, 2, 3, 4, 5, 6, 7, 8, 9]. The complexity of these phenomena and the difficulty of performing simple laboratory-scale experiments explain why progress in this field has been slow for a long time since. Recently, the development of smaller annular chambers in laboratories has opened the path to investigate flow fields [10, 11], ignition [12], flame response to acoustics [13] as well as azimuthal instabilities in these configurations [4, 14, 15]. At the same time, theoretical and numerical approaches have progressed in three directions: (1) full 3D LES of annular chambers have been developed [16, 17], (2) 3D acoustic tools have been adapted to annular chambers [18, 19, 20, 21] and (3) analytical approaches have been proposed to avoid the costs of 3D formulations and allow to investigate the stability and control of modes at low cost [5, 22, 23]. This last class of approach is especially interesting to elucidate mechanisms (such as transverse forcing effect [23], symmetry breaking [5] and mode nature [24]) because they can provide explicit solutions for the frequency and the growth rate of all modes. The difficulty in these methods is to be able to construct a model which can be handled by simple analytical approaches while retaining most of the important physical phenomena and geometrical specificities of annular chambers.

One interesting issue in studies of instabilities in annular chambers is to classify them. For example, standing and turning modes [1, 24] are both observed [1, 5, 17, 25] but predicting which mode type will appear in practice and whether they can be studied and controlled with the same method remains difficult [23]. Similarly, most large scale annular chambers exhibit multiple acoustic modes in the frequency range of interest (typically 10 to 30 acoustic modes can be identified in a large scale industrial chamber between 0 and 300 Hz) and classifying them into categories is the first step to control them. These categories are typically 'longitudinal vs azimuthal modes' or 'modes involving only a part of the chamber (decoupled modes) vs modes involving the whole system (coupled modes)' [1, 3, 20, 21]. Knowing that a given unstable mode is controlled only by a certain part of the combustor is an obvious asset for any control strategy. In the case of combustors including an annular plenum, burners and an annular chamber, such a classification is useful for example to understand how azimuthal modes in the plenum and

in the chamber (which have a different radius and sound speed and therefore different frequencies) can interact or live independently. For example, FEM simulations of a real industrial gas turbine [20] produce numerous complex modes which involve several cavities (plenum, burners and chamber) at the same time. Unfortunately determining whether certain parts of a chamber can be 'decoupled' from the rest of the chamber is a task for which there is no clear strategy. 'Decoupling' factors have been derived for longitudinal modes in academic burners where all modes are longitudinal [26]. Extending these approaches to annular systems requires first to derive analytical solutions allowing to isolate the effect of parameters on the modes structure. This is one of the objectives of this paper.

Noiray et al. [5] and Ghirardo and Juniper [23] have proposed analytical analysis of complex non-linear mechanisms but only on simple configurations where the combustor is modeled with an annular rig alone. Parmentier et al [22] have derived an analytical method called ATACAMAC (for Analytical Tool to Analyze and Control Azimuthal Modes in Annular Combustors) for a more realistic configuration called BC (N Burners + Chamber) (Fig.1 left). By describing acoustic wave propagation and flame action in a network of ducts representing the BC configuration and introducing a reduction method for the overall system corresponding to wave propagation in this network, they were able to predict the frequencies and growth rate of azimuthal and longitudinal modes, to identify their nature and predict their response to passive control methods such as symmetry breaking. Stow and Dowling [27] also investigated BC configurations with low-order models and focused on limit-cycles by introducing more complex flame models (by adding non-linearities and uniform spread of convection times).

However, BC geometries did not correspond exactly to real annular chambers where the N burners are connected not only downstream (to the combustion chamber) but also upstream to the plenum which feeds them. PBC configurations (Plenum + N Burners + Chamber) (Fig.1 right) have been proved [1, 20] to correctly reproduce the behavior of complex industrial annular combustors (Fig. 2). Evesque and Polifke [8] studied PBC configurations using both FEM simulations and low-order models. Pankiewicz and Sattelmayer [21] also investigated this case using time-domain simulations with an axial mean flow. Both the linear and non-linear flames regimes are studied by introducing saturations in the Flame Transfer Functions. They pointed out that the time-delay of the FTF plays a crucial role for predicting the frequency as well as the nature of azimuthal modes in such a configuration.

Thus, no full analytical resolution of frequency and nature of azimuthal modes have been performed in PBC configurations. The present paper extends the analytical methodology of Schuller et al. [26] for longitudinal tubes and of Parmentier et al [22] for BC configurations to a PBC configuration with N burners in order to highlight key parameters involved in the coupling mechanisms.

In most network approaches for combustion instabilities, a very large matrix is built to describe the acoustics of the system [8, 26, 28]. Here, we introduce a significantly simpler methodology called ANR (Annular Network Reduction) which allows to reduce the size of the acoustic problem in an annular system to a simple 4-by-4 matrix containing all information of the combustor resonant modes. This method allows to obtain explicit dispersion relations for PBC configurations and to exhibit the exact forms of the coupling parameters for azimuthal modes between the plenum and the burners on one hand and between the burners and the chamber on the other hand.

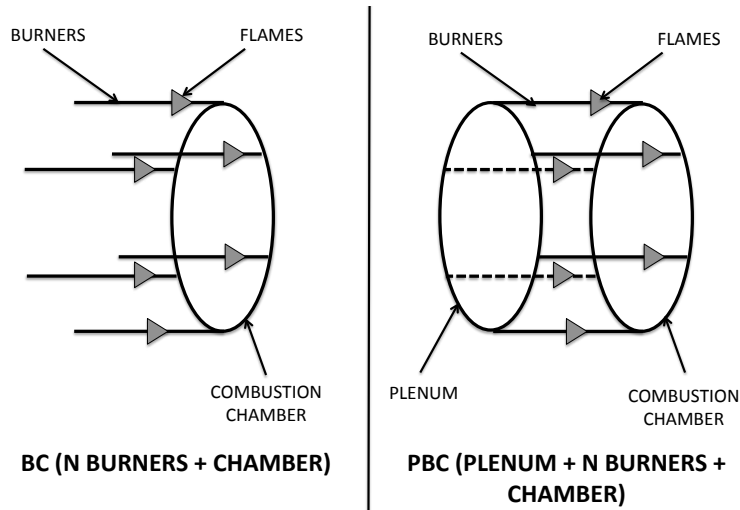


Figure 1: Configurations to study unstable modes in annular chambers

The paper is organized as follows: Section 2 describes the principle of the ANR (Annular Network Reduction) methodology and the submodels to account for active flames. The decomposition of the network into H-shaped connectors and azimuthal propagators allows to build an explicit dispersion relation giving the frequency, growth rate and structure of all modes. In Section 3, thermoacoustic regimes (from fully decoupled to strongly coupled)

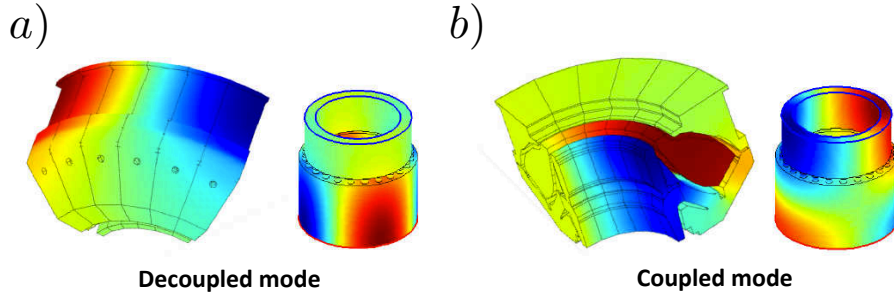


Figure 2: FEM simulations performed by Campa et al. [20] on a complex industrial gas turbine (only 6 sectors are displayed) and its PBC configuration model. Two kinds of eigenmodes are observed: a) Decoupled mode and b) Coupled mode

are defined depending on the analytical coupling parameters conducted in Section 2. Finally, this analytical model is validated using the model annular chamber described in Section 4 with simplistic shapes to construct coupling factors and study azimuthal modes for a case where a plenum is connected to a chamber by four similar burners ($N = 4$). First the weakly coupled regime (Section 5) and then the strongly coupled regime (Section 6) are investigated. The bifurcation [29] from weakly to strongly coupled situations is triggered by increasing the flame interaction index controlling the flame response to the acoustic flow. Results show that ATACAMAC allows to predict azimuthal turning and standing modes in a PBC configuration and performs as well as a 3D Helmholtz solver for all three regimes while simple annular rigs [5, 23] or BC models [22, 27] are not able to capture the bifurcation from weakly to strongly coupled regimes.

2. A network model for PCB (Plenum+Burners+Chamber) configurations

2.1. Model description

The model is based on a network view of the annular chamber fed by burners connected to an annular plenum (Fig. 3). This model is limited to situations where pressure fluctuations depend on the angle θ (or x) but not on z in the chamber and the plenum (they depend on the coordinate z only in the N burners). This case can be observed in combustors terminated in choked nozzles which behave almost like a rigid wall (i.e. $w' = 0$ under the

low upstream Mach number assumption [30]). Note however that this restriction prevents the present model to represent academical combustors where the combustion chamber is open to the atmosphere [4, 14, 15] or to predict "mixed modes" appearing at higher frequencies in configurations terminated by choked nozzles [20].

Since the chamber inlet is also close to a velocity node, modes which have no variation along z can develop in the chamber, as shown by recent LES [31]. Radial modes (where p' depends on r) are neglected because often occurring at high frequency. Gas dynamics are described using standard linearized acoustics for perfect gases in the low Mach number approximation. The mean flow induced by swirlers remains slow [31] and azimuthal waves propagate at the sound speed which is different in the plenum (fresh gas at sound speed c_u^0) and the chamber (burnt gas at sound speed c^0).

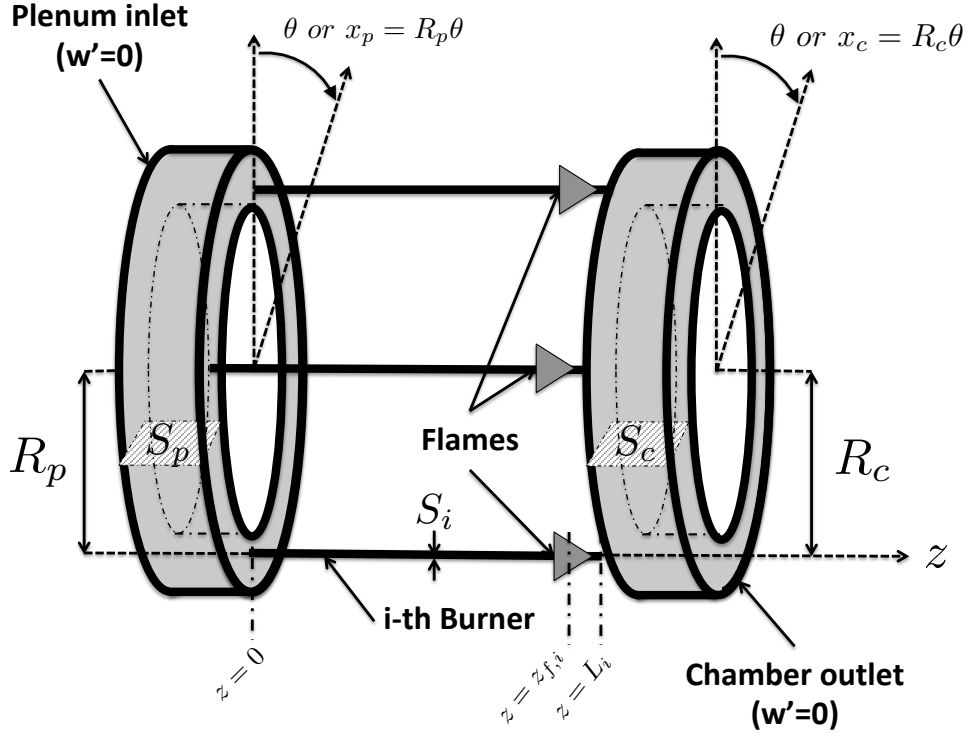


Figure 3: Network representation of the plenum, burners and chamber (PBC configuration)

In the initial ATACAMAC study of Parmentier et al. [22], a BC (Burners+Chamber) configuration was considered: an annular chamber is fed by

N burners without taking into account the existence of a plenum ; the impedance imposed at the inlet of the N burners corresponded to a closed end ($w' = 0$) and flames were located at the burners extremity ($z_{f,i} \simeq L_i$ where L_i is the length of the i^{th} burner). This section describes how this BC case is extended to PBC (Plenum+Burners+Chamber) configurations where an annular plenum feeds N ducts ("burners") which are all connected to an annular chamber. Most annular gas turbine chambers can be modeled using this scheme (Fig. 3).

In a PBC configuration, burners are connected at both ends to the annular plenum and chamber. The boundary conditions $w' = 0$ used for BC configurations are retained here only on walls of the annular cavities but not at the inlet/outlet sections of the burners. Mean density in the annular chamber is noted ρ^0 (ρ_u^0 in the plenum). The subscript u stands for unburnt gases. The perimeter and the section of the annular plenum are noted $2L_p = 2\pi R_p$ and S_p respectively while L_i and S_i stand for the length and cross section area of the i^{th} burner. The perimeter and the section of the annular chamber are noted $2L_c = 2\pi R_c$ and S_c respectively. The position along the annular plenum and chamber is given by the angle θ defining abscissa $x_p = R_p\theta$ for the plenum and $x_c = R_c\theta$ for the chamber. The location of the flames in the burners is given by the normalized abscissa $\alpha = z_{f,i}/L_i$ (Fig. 3).

2.2. Acoustic waves description and ANR methodology

To reduce the size of the system, a new methodology called ANR (Annular Network Reduction) is proposed to extract only useful information of azimuthal modes of the resonant combustor. First, the combustor is decomposed into N sectors (Fig. 4) by assuming that every sector can be studied separately and that no flame-to-flame interaction occurs between neighboring sectors, a question which is still open today [32, 33]. Staffelbach et al. [31] have shown that this was the case in LES of azimuthal modes. Worth and Dawson [4, 34] have also demonstrated experimentally that this assumption in annular combustor is valid when the distance between burners is large enough to avoid flames merging.

For each individual sector, the acoustic problem may be split into two parts: propagation (Section 2.2.1 and already described in [22, 35, 36]) and H-shaped connector (Section 2.2.2) (Fig. 5). The angle θ and the coordinates of the plenum x_p and chamber x_c take their origin at the burner i . The end of the sector i is located at $x_p = \frac{2L_p}{N}$ and $x_c = \frac{2L_c}{N}$ (thus assuming that burners

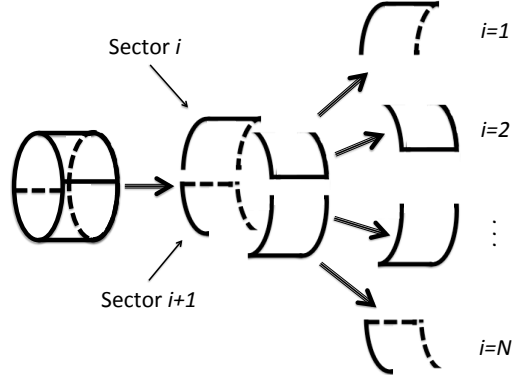


Figure 4: Decomposition of an annular combustor in N sectors

are evenly located around the annular combustor). H-shaped connectors are supposed to be compact regarding the acoustic wavelength.

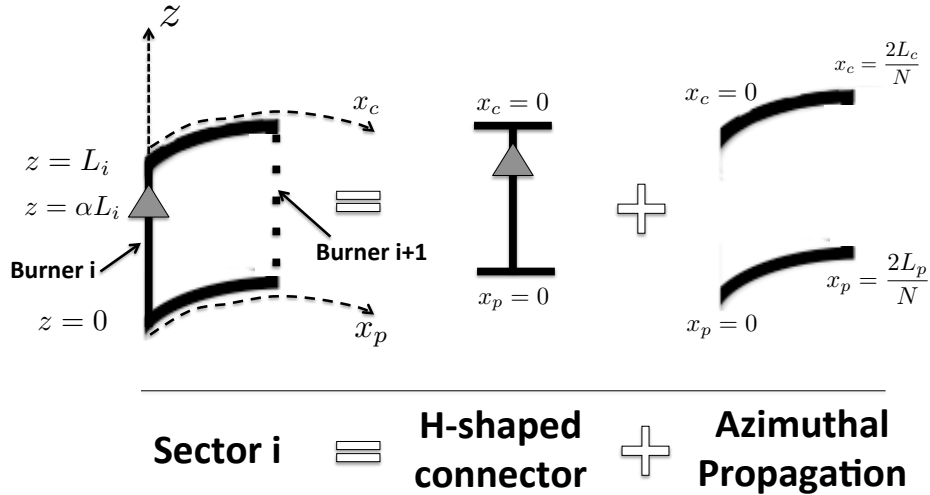


Figure 5: ANR methodology: splitting of one sector into propagation and H-shaped section parts for a PBC configuration

2.2.1. Propagation

There are two main paths to analyze azimuthal modes in annular chambers with simple models: the first one is to write the mode explicitly as a function of the azimuthal angle θ as done in [7, 8]

for example. The second approach is to use a network discretization along the azimuthal direction [1, 22]. An advantage of the first method is the capability of considering modes which are azimuthal but also involve an axial dependence, something which can not be done yet with the second approach. However, the second method describes explicitly the coupling between annular cavities and burners and therefore has been applied here for ATACAMAC.

Assuming linear acoustics, the pressure and velocity perturbations inside the i^{th} sector of the annular chamber (denoted via the subscript c, i) can be written as:

$$p'_{c,i}(x_c, t) = (A_i \cos(kx_c) + B_i \sin(kx_c))e^{-j\omega t} \quad (1)$$

$$\rho^0 c^0 u'_{c,i}(x_c, t) = j(A_i \sin(kx_c) - B_i \cos(kx_c))e^{-j\omega t} \quad (2)$$

where $j^2 = -1$, $k = \omega/c^0$ is the wavenumber, A_i and B_i are complex constants.

From Eqs. (1) and (2), pressure and velocity perturbations at two positions in the chamber x_{c0} and $x_{c0} + \Delta x_c$ are linked by:

$$\begin{bmatrix} p'_{c,i} \\ \frac{1}{j}\rho^0 c^0 u'_{c,i} \end{bmatrix}_{(x_{c0}+\Delta x_c, t)} = \underbrace{\begin{bmatrix} \cos(k\Delta x_c) & -\sin(k\Delta x_c) \\ \sin(k\Delta x_c) & \cos(k\Delta x_c) \end{bmatrix}}_{R(k\Delta x_c)} \begin{bmatrix} p'_{c,i} \\ \frac{1}{j}\rho^0 c^0 u'_{c,i} \end{bmatrix}_{(x_{c0}, t)} \quad (3)$$

The matrix $R(k\Delta x_c)$ is a 2D rotation matrix of angle $k\Delta x_c$. In the case where N burners are equally distributed over the annular chamber, the propagation in the chamber between each burner is fully described by the transfer matrix $R(k\frac{2L_c}{N})$ where $2L_c$ is the chamber perimeter.

Wave propagation in the i^{th} sector of the plenum satisfies the same equation than in the chamber Eq. (3) if the sound speed in fresh gases c_u^0 is used:

$$\begin{bmatrix} p'_{p,i} \\ \frac{1}{j}\rho_u^0 c_u^0 u'_{p,i} \end{bmatrix}_{(x_0+\Delta x_p, t)} = \underbrace{\begin{bmatrix} \cos(k_u\Delta x_p) & -\sin(k_u\Delta x_p) \\ \sin(k_u\Delta x_p) & \cos(k_u\Delta x_p) \end{bmatrix}}_{R(k_u\Delta x_p)} \begin{bmatrix} p'_{p,i} \\ \frac{1}{j}\rho_u^0 c_u^0 u'_{p,i} \end{bmatrix}_{(x_0, t)} \quad (4)$$

where $k_u = \omega/c_u^0$.

Propagation in the i^{th} burner from the plenum ($z = 0$) to the flame ($z = \alpha L_i$) and from $z = \alpha L_i$ to $z = L_i$ (Fig. 6) can be described in the same

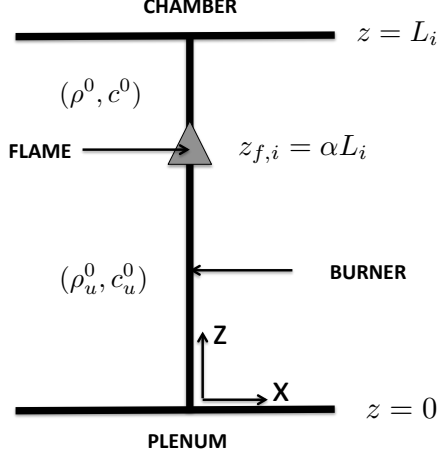


Figure 6: Propagation in the i^{th} burner for a PBC configuration in the ANR method

way considering propagation in fresh gases for the first part ($0 < z < \alpha L_i$) and hot gases in the second part ($\alpha L_i < z < L_i$):

Therefore, equations for the wave propagation in the i^{th} burner are:

$$\begin{bmatrix} p'_i \\ \frac{1}{j} \rho_u^0 c_u^0 w'_i \end{bmatrix}_{(\alpha L_i, t)} = R(k_u \alpha L_i) \begin{bmatrix} p'_i \\ \frac{1}{j} \rho_u^0 c_u^0 w'_i \end{bmatrix}_{(0, t)} \quad (5)$$

and

$$\begin{bmatrix} p'_i \\ \frac{1}{j} \rho^0 c^0 w'_i \end{bmatrix}_{(L_i, t)} = R(k(1 - \alpha) L_i) \begin{bmatrix} p'_i \\ \frac{1}{j} \rho^0 c^0 w'_i \end{bmatrix}_{(\alpha L_i, t)} \quad (6)$$

2.2.2. H-shaped connector

The physical parameters at the entrance (located at the end of the $i - 1^{\text{th}}$ sector corresponding to $\theta = \frac{2\pi}{N}$ and consequently $x_p = \frac{2L_p}{N}$ and $x_c = \frac{2L_c}{N}$) must be linked to the output parameters (corresponding to the beginning of the i^{th} sector located at $\theta = 0$ and consequently $x_p = x_c = 0$) as shown in Fig. 7.

The H-shaped connectors are treated as compact elements in the azimuthal direction. Jump conditions are first written along the x direction at $z = 0$ and $z = L_i$: at low Mach number [2], they correspond to the continuity of pressure and volume rate through the interface. For the sake of simplicity, more complex interactions (e.g. effective length or pressure drop effects) [20]

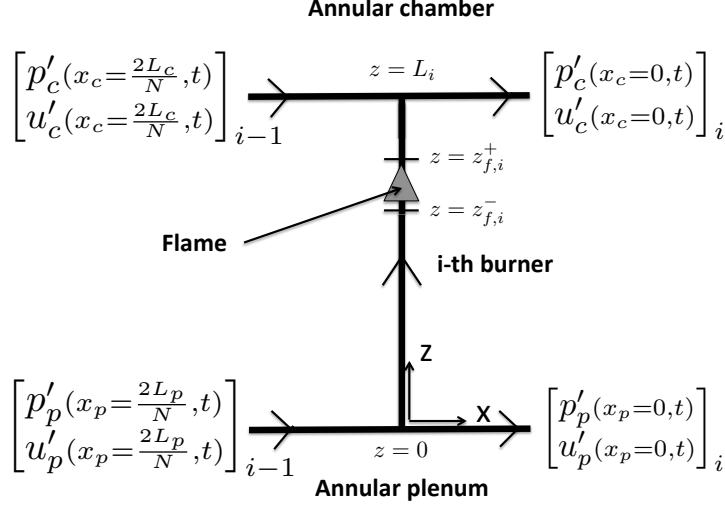


Figure 7: H-shaped overview in the ANR method

are neglected knowing they could affect the coupling mechanisms between cavities. At $z = L_i$:

$$p'_{c,i-1}(x_c = \frac{2L_c}{N}, t) = p'_{c,i}(x_c = 0, t) = p'_i(z = L_i) \quad (7)$$

$$S_c u'_{c,i-1}(x_c = \frac{2L_c}{N}, t) + S_i w'_i(z = L_i) = S_c u'_{c,i}(x_c = 0, t) \quad (8)$$

and at $z = 0$:

$$p'_{p,i-1}(x_p = \frac{2L_p}{N}, t) = p'_{p,i}(x_p = 0, t) = p'_i(z = 0) \quad (9)$$

$$S_p u'_{p,i-1}(x_p = \frac{2L_p}{N}, t) = S_i w'_i(z = 0) + S_p u'_{p,i}(x_p = 0, t) \quad (10)$$

Jump conditions are also required in the burners through the flames located at $z = z_{f,i}$. They are assumed to be planar and compact: their thickness is negligible compared to the acoustic wavelength. Flames are located at $z = z_{f,i}^+ = z_{f,i}^- \simeq \alpha L_i$ where superscripts $+$ and $-$ denote the downstream and upstream positions of the i^{th} flame. At low Mach number, jump conditions through the flame imply equality of pressure and flow rate discontinuity due to an extra volume source term related to unsteady combustion [2]:

$$p'_i(z_{f,i}^+) = p'_i(z_{f,i}^-) \quad (11)$$

$$S_i w'_i(z_{f,i}^+) = S_i w'_i(z_{f,i}^-) + \frac{\gamma_u - 1}{\gamma_u P^0} \dot{\Omega}'_{T,i} \quad (12)$$

where P^0 is the mean pressure and γ_u is the heat capacity ratio of fresh gases. The unsteady heat release $\dot{\Omega}'_{T,i}$ is expressed using the FTF model (Flame Transfer Function) [37]:

$$\frac{\gamma_u - 1}{\gamma_u P^0} \dot{\Omega}'_{T,i} = S_i n_i e^{j\omega\tau_i} w'_i(z_{f,i}^-) \quad (13)$$

where the interaction index n_i ¹ and the time-delay τ_i are input data (depending on frequency) describing the interaction of the i^{th} flame with acoustics. Therefore, the jump condition in Eq. (12) is recast using Eq. (13):

$$S_i w'_i(z_{f,i}^+) = S_i (1 + n_i e^{j\omega\tau_i}) w'_i(z_{f,i}^-) \quad (14)$$

Thanks to Eqs. (7 - 14), a transfer matrix T_i of the H-shaped connector of Fig. 7 is defined as:

$$\begin{bmatrix} p'_p(x_p=0,t) \\ \frac{1}{j}\rho_u^0 c_u^0 u'_p(x_p=0,t) \\ p'_c(x_c=0,t) \\ \frac{1}{j}\rho^0 c^0 u'_c(x_c=0,t) \end{bmatrix}_i = T_i \begin{bmatrix} p'_p(x_p=\frac{2L_p}{N},t) \\ \frac{1}{j}\rho_u^0 c_u^0 u'_p(x_p=\frac{2L_p}{N},t) \\ p'_c(x_c=\frac{2L_c}{N},t) \\ \frac{1}{j}\rho^0 c^0 u'_c(x_c=\frac{2L_c}{N},t) \end{bmatrix}_{i-1} \quad (15)$$

where the transfer matrix T_i is:

$$T_i = I_d + 2 \begin{bmatrix} 0 & 0 & 0 & 0 \\ \Gamma_{i,1} & 0 & \Gamma_{i,2} & 0 \\ 0 & 0 & 0 & 0 \\ \Gamma_{i,3} & 0 & \Gamma_{i,4} & 0 \end{bmatrix} \quad (16)$$

and the coefficients $\Gamma_{i,k}$, $k = 1$ to 4 are:

$$\Gamma_{i,1} = -\frac{1}{2} \frac{S_i \cos(k(1-\alpha)L_i) \cos(k_u \alpha L_i) - \mathbb{F} \sin(k(1-\alpha)L_i) \sin(k_u \alpha L_i)}{S_p \cos(k(1-\alpha)L_i) \sin(k_u \alpha L_i) + \mathbb{F} \sin(k(1-\alpha)L_i) \cos(k_u \alpha L_i)} \quad (17)$$

¹Typical values of the interaction index n_i can reach $T_b/T_u - 1$ at low frequency.

$$\Gamma_{i,2} = \frac{1}{2} \frac{S_i}{S_p} \frac{1}{\cos(k(1-\alpha)L_i) \sin(k_u \alpha L_i) + \mathbb{F} \sin(k(1-\alpha)L_i) \cos(k_u \alpha L_i)} \quad (18)$$

$$\Gamma_{i,3} = \frac{1}{2} \frac{S_i}{S_c} \frac{\mathbb{F}}{\cos(k(1-\alpha)L_i) \sin(k_u \alpha L_i) + \mathbb{F} \sin(k(1-\alpha)L_i) \cos(k_u \alpha L_i)} \quad (19)$$

$$\Gamma_{i,4} = -\frac{1}{2} \frac{S_i}{S_c} \frac{\mathbb{F} \cos(k(1-\alpha)L_i) \cos(k_u \alpha L_i) - \sin(k(1-\alpha)L_i) \sin(k_u \alpha L_i)}{\cos(k(1-\alpha)L_i) \sin(k_u \alpha L_i) + \mathbb{F} \sin(k(1-\alpha)L_i) \cos(k_u \alpha L_i)} \quad (20)$$

with the flame parameter \mathbb{F} :

$$\mathbb{F} = \frac{\rho^0 c^0}{\rho_u^0 c_u^0} (1 + n e^{j\omega\tau}) \quad (21)$$

These coefficients are the coupling parameters for PBC configurations. $\Gamma_{i,1}$ and $\Gamma_{i,2}$ are linked to the plenum/burner junction (depending on S_i/S_p which measures the ratio between the burner section S_i and the plenum section S_p) while $\Gamma_{i,3}$ and $\Gamma_{i,4}$ are linked to the chamber/burner junction (depending on S_i/S_c which measures the ratio of the burner section to the chamber section (Fig. 3)).

2.3. Dispersion relation calculation given by the ANR method

In previous sections, the overall problem has been split into smaller parts and now has to be reconstructed in order to obtain the dispersion relation for the whole system. First, the pressure and velocity fluctuations at the end of the $i-1^{th}$ sector are linked to those at the end of the i^{th} sector using Eqs. (3), (4) and (15).

$$\begin{bmatrix} p'_p(x_p=\frac{2L_p}{N}, t) \\ \frac{1}{j} \rho_u^0 c_u^0 u'_p(x_p=\frac{2L_p}{N}, t) \\ p'_c(x_c=\frac{2L_c}{N}, t) \\ \frac{1}{j} \rho^0 c^0 u'_c(x_c=\frac{2L_c}{N}, t) \end{bmatrix}_i = R_i \begin{bmatrix} p'_p(x_p=0, t) \\ \frac{1}{j} \rho_u^0 c_u^0 u'_p(x_p=0, t) \\ p'_c(x_c=0, t) \\ \frac{1}{j} \rho^0 c^0 u'_c(x_c=0, t) \end{bmatrix}_i = R_i T_i \begin{bmatrix} p'_p(x_p=\frac{2L_p}{N}, t) \\ \frac{1}{j} \rho_u^0 c_u^0 u'_p(x_p=\frac{2L_p}{N}, t) \\ p'_c(x_c=\frac{2L_c}{N}, t) \\ \frac{1}{j} \rho^0 c^0 u'_c(x_c=\frac{2L_c}{N}, t) \end{bmatrix}_{i-1} \quad (22)$$

where T_i is the matrix defined in Eq. (16) and R_i is the propagation matrix inside the plenum and chamber in the i^{th} sector defined by:

$$R_i = \begin{bmatrix} R(k_u \frac{2L_p}{N}) & 0 & 0 \\ 0 & 0 & 0 \\ 0 & 0 & R(k \frac{2L_c}{N}) \end{bmatrix} \quad (23)$$

where $R(k_u \frac{2L_p}{N})$ and $R(k \frac{2L_c}{N})$ are 2-by-2 matrices defined in Eqs. (3) and (4)

Then, Eq. (22) can be repeated through the N sectors and periodicity imposes that:

$$\begin{bmatrix} p'_p(x_p=\frac{2L_p}{N},t) \\ \frac{1}{j}\rho_u^0 c_u^0 u'_p(x_p=\frac{2L_p}{N},t) \\ p'_c(x_c=\frac{2L_c}{N},t) \\ \frac{1}{j}\rho^0 c^0 u'_c(x_c=\frac{2L_c}{N},t) \end{bmatrix}_{i=1} = \left(\prod_{i=N}^1 R_i T_i \right) \begin{bmatrix} p'_p(x_p=\frac{2L_p}{N},t) \\ \frac{1}{j}\rho_u^0 c_u^0 u'_p(x_p=\frac{2L_p}{N},t) \\ p'_c(x_c=\frac{2L_c}{N},t) \\ \frac{1}{j}\rho^0 c^0 u'_c(x_c=\frac{2L_c}{N},t) \end{bmatrix}_{i=1} \quad (24)$$

System Eq. (24) leads to non-null solutions if and only if its determinant is null:

$$\det \left(\prod_{i=N}^1 R_i T_i - I_d \right) = 0 \quad (25)$$

where I_d is the 4-by-4 identity matrix and the matrix $M = \prod_{i=N}^1 R_i T_i$ is the transfer matrix of the overall system. Eq. (25) provides an implicit equation for the pulsation ω and gives the stability limits and the frequency of unstable modes. Note that Eq. (25) given by the ANR methodology only involves a 4-by-4 determinant² irrespective of the number of burners N .

3. Analytical procedure and coupling limits

Due to significant non linearities, Eq. (25) cannot be solved analytically in the general case. However different situations (Fig. 8) can be exhibited where Eq. (25) can be solved depending on values taken by the coupling parameters $\wp_{p,i}$ and $\wp_{c,i}$:

$$\wp_{p,i} = \max(|\Gamma_{i,1}|, |\Gamma_{i,2}|) \quad (26)$$

and

$$\wp_{c,i} = \max(|\Gamma_{i,3}|, |\Gamma_{i,4}|) \quad (27)$$

The parameters $\wp_{p,i}$ and $\wp_{c,i}$ measure the coupling effect of the plenum/burner junction and the chamber/burner junction respectively for the i^{th} sector.

²The ANR methodology retains only useful information related to azimuthal modes of the annular cavities. Knowing that these modes are a combination of two characteristic waves, the minimum size of the matrix system is $2\mathcal{C}$ -by- $2\mathcal{C}$ where \mathcal{C} is the number of annular cavities (here $\mathcal{C} = 2$: plenum + chamber)

They depend only on the geometry (section ratios S_i/S_p and S_i/S_c as well as the burners length L_i) and the flame (the flame interaction factor \mathbb{F} and the flame position α). Longitudinal modes in the burners can be obtained with this model but only purely azimuthal modes will be studied in this paper (Fig. 8).

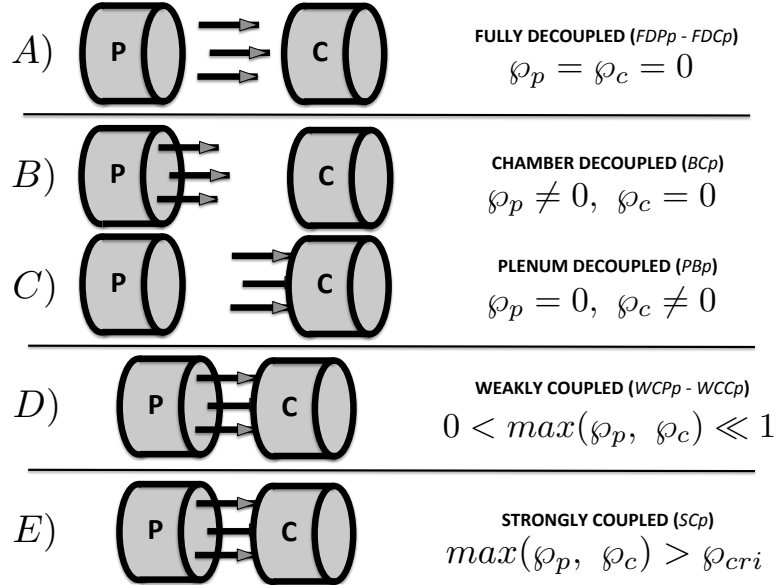


Figure 8: The four coupling situations depending on the parameters \wp_p and \wp_c

3.1. Fully decoupled situations (FDPp and FDCp)

If the coupling parameters have vanishing small values ($\wp_{p,i} = 0$ and $\wp_{c,i} = 0$), the coupling matrices of each sector (T_i in Eq. (25)) are the identity matrix. As a consequence, the dispersion relation (Eq. (25)) reduces to:

$$\det \left(\prod_{i=N}^1 R_i - I_d \right) = 0 \quad (28)$$

The matrices R_i being block matrices of 2-by-2 rotation matrices which

satisfy $R(\theta_1)R(\theta_2) = R(\theta_1 + \theta_2)$, Eq. (28) becomes:

$$\begin{aligned} \det \left(\prod_{i=N}^1 R_i - I_d \right) &= \det \left(\begin{bmatrix} R(2k_u L_p) - I_d & 0 & 0 \\ 0 & 0 & 0 \\ 0 & 0 & R(2k L_c) - I_d \end{bmatrix} \right) \\ &= \det(R(2k_u L_p) - I_d) \det(R(2k L_c) - I_d) = 0 \quad (29) \end{aligned}$$

Solutions of Eq. (29) are $k_u L_p = p\pi$ and $k L_c = p\pi$ where p is an integer. They correspond to two families of modes which live separately (case A in Fig. 8):

- **FDPp - Fully Decoupled Plenum mode of order p:** they satisfy the relation $k_u L_p = p\pi$ and correspond to the azimuthal modes of the annular plenum alone (Fig. 8).
- **FDCp - Fully Decoupled Chamber mode of order p:** they satisfy the relation $k L_c = p\pi$ and correspond to the azimuthal modes of the annular chamber alone (Fig. 8).

3.2. Chamber or plenum decoupled situations (PBp and BCp)

These situations correspond to cases where either the plenum or the chamber are fully decoupled from the burners, i.e. respectively $\varphi_p = 0$ or $\varphi_c = 0$ (cases B and C in Fig. 8). The transfer matrices of each sector are block-triangular leading to a simple relation for the determinant and consequently for the dispersion relation (Eq. 25) without assumption on the non-null parameter φ_p or φ_c . As for the fully decoupled situations, two families of modes can be exhibited (cases B and C in Fig. 8):

- **PBp - Plenum/Burners mode of order p:** in this situation, $\varphi_c = 0$. The annular chamber is fully decoupled from the system (burners+plenum) and the dispersion relation Eq. (25) reduces to two equations:

$$\det(R(2k L_c) - 1) = 0 \quad (30)$$

$$\det \left(\prod_{i=N}^1 R \left(\frac{2k_u L_p}{N} \right) \begin{bmatrix} 1 & 0 \\ \Gamma_{i,1} & 1 \end{bmatrix} - I_d \right) = 0 \quad (31)$$

Eq. (30) corresponds to the dispersion relation of a FDCp mode while Eq. (31) is the dispersion relation of a PB (Plenum + Burners) configuration where an impedance $Z = 0$ is imposed at the downstream end of the burner simulating the large chamber decoupled from the system (case B in Fig. 8). This latter mode is referred to as "PBp" standing for Plenum/Burners mode of order p. These situations are, however, unrealistic because they neglect all interactions between the annular plenum and chamber: the only solution to obtain $\varphi_c \rightarrow 0$ in a PBC configuration is an infinite cross section of the chamber ($S_c \rightarrow \infty$ in Eqs. (19 - 20)). Therefore, this paper will focus on other situations (e.g. cases D and E in Fig. 8) which are more representative of real engines by including the interaction between annular cavities.

- **BCp - Burners/Chamber mode of order p:** in this situation, $\varphi_p = 0$ so that the annular plenum is fully decoupled from the rest of the system and the dispersion relation Eq. (25) reduces to two equations:

$$\det(R(2k_u L_p) - 1) = 0 \quad (32)$$

$$\det\left(\prod_{i=N}^1 R\left(\frac{2kL_c}{N}\right) \begin{bmatrix} 1 & 0 \\ \Gamma_{i,4} & 1 \end{bmatrix} - I_d\right) = 0 \quad (33)$$

The first equation (Eq. (32)) is the dispersion relation of a FDPp mode while Eq. (33) is the dispersion relation of a BC (Burners + Chamber) configuration where a pressure node ($Z = 0$) is imposed at the upstream end of the burner modeling the large plenum decoupled from the burners and the annular chamber (case C in Fig. 8). This latter mode is called "BCp" for Burners/Chamber mode of order p and was already studied by Parmentier et al. [22].

3.3. Weakly coupled situations (WCPp and WCCp)

When φ_p and φ_c are both non zero, both azimuthal modes of the plenum and the chamber can exist and interact through the burners. If φ_p and φ_c remain small (Eq. (34)), an asymptotic solution can be constructed.

$$\forall i, 0 < \varphi_{p,i} \ll 1 \text{ and } 0 < \varphi_{c,i} \ll 1 \quad (34)$$

The parameters $\wp_{p,i}$ (Eq. 26) and $\wp_{c,i}$ (Eq. 27) measure the strength of the coupling effect of the plenum/burner junction and the chamber/burner junction respectively for the i^{th} sector. If they are small, the transfer matrices of each sector ($T_i R_i$ in Eq. (25)) are close to the rotation matrix R_i defined in Eq. (4) so that the eigenfrequencies of the system will be close to a FDPp or a FDCp mode. Consequently, as for fully decoupled modes, two families of modes can be exhibited (case D in Fig. 8):

- **WCPp - Weakly Coupled Plenum mode of order p:** this mode is close to a FDPp mode and the solution for the wavenumber k_u can be searched as an expansion around this case:

$$k_u L_p = p\pi + \epsilon_p \quad (35)$$

where $\epsilon_p \ll p\pi$

- **WCCp - Weakly Coupled Chamber mode of order p:** this mode is close to a FDCp mode and the solution for the wavenumber k can be searched as an expansion around this case:

$$k L_c = p\pi + \epsilon_c \quad (36)$$

where $\epsilon_c \ll p\pi$

For weakly coupled modes, this low coupling assumption allows a Taylor expansion of the dispersion relation (Eq. 25) which can be truncated and solved providing analytical solutions for ϵ_c and ϵ_p . This expansion is case-dependent: the $N = 4$ case will be detailed in Section. 5. Basically, results show that azimuthal modes will be either Chamber or Plenum modes slightly modified by their interaction with the rest of the combustor.

Note that the low coupling assumption ($\wp_{p,i} \ll 1$ and $\wp_{c,i} \ll 1$) does not imply low thermo-acoustic coupling ($n_i \ll 1$) because surface ratios between burner and plenum or chamber are usually small ($S_i/S_c \ll 1$ and $S_i/S_p \ll 1$).

In the specific configuration where the flames are located at the end of the burner ($\alpha = z_{f,i}/L_i = 1$ in Fig. 3), however, the coupling parameters

simplify as:

$$\Gamma_{i,1} = -\frac{1}{2} \frac{S_i}{S_p} \cotan(k_u L_i) \quad (37)$$

$$\Gamma_{i,2} = \frac{1}{2} \frac{S_i}{S_p} \frac{1}{\sin(k_u L_i)} \quad (38)$$

$$\Gamma_{i,3} = \frac{1}{2} \frac{S_i}{S_c} \frac{\mathbb{F}}{\sin(k_u L_i)} \quad (39)$$

$$\Gamma_{i,4} = -\frac{1}{2} \frac{S_i}{S_c} \mathbb{F} \cotan(k_u L_i) \quad (40)$$

where \mathbb{F} is the flame parameter defined in Eq. (21). Eq. (37) to (40) correspond to an extension of the coupling parameters proposed by Palies and Schuller [26] for longitudinal instabilities and Parmentier et al. [22] for azimuthal instabilities in a BC configuration. They show that decoupling ($\wp_{p,i} \ll 1$ and $\wp_{c,i} \ll 1$) can be expected in this case for small sections ratios $S_i/S_p \ll 1$ and $S_i/S_c \ll 1$, when the flame parameter \mathbb{F} (Eq. (21)) is small too.

3.4. Strongly coupled situations (SCp)

The low coupling assumption ($\wp_{p,i} \ll 1$ and $\wp_{c,i} \ll 1$) is not valid at high flame interaction factor ($\mathbb{F} = \frac{\rho^0 c^0}{\rho_u^0 c_u^0} (1 + ne^{j\omega\tau})$) or high surface ratios (S_i/S_p or S_i/S_c). In these situations (case E in Fig. 8), a numerical resolution of the analytical dispersion relation (Eq. (25)) is required. It can be achieved by a non-linear solver based on the Newton-Raphson algorithm.

No rule already exists to distinguish a weakly or strongly coupled situation for real engines (characterized by an unknown critical parameter \wp_{crit} , Fig. 8). Moreover, classifying modes in two families as it is the case for fully decoupled situations (FDPp and FDCp modes), plenum or chamber decoupled situations (PBp and BCp modes) and weakly decoupled situations (WCPp and WCCp modes) is not possible anymore due to the interaction between all parts of the system. A first attempt to identify key parameters and rules to differentiate weakly and strongly coupled situations is described in Section 6.

In the remaining of the paper, the weakly and strongly coupled situations (Fig.8) will be studied on the PBC configuration with four burners ($N = 4$) described in Section 4. The transition from weakly (Section 5) to strongly coupled (Section 6) regimes is controlled by a critical coupling limit factor

\wp_{crit} . The transition occurs when $max(\wp_p, \wp_c) > \wp_{crit}$. The geometry being fixed (Table 1) and the coupling parameters (\wp_p and \wp_c) depending only on the geometry and the flame, the transition will be triggered by increasing the flame interaction index n_i of the flames from $n_i = 1.57$ (weak coupling) to $n_i = 8.0$ (strong coupling).

4. Validation in a simplified model chamber

Eigenfrequencies and mode structures of the analytical resolution of the dispersion relation under the low coupling factors assumption (Fig. 8, all modes except SCp) are first compared to a full 3D acoustic code and to the direct resolution of Eq. (25) in the case of a simplified 3D PBC configuration which is used as a toy-model for ATACAMAC and corresponds to a typical industrial gas turbine.

4.1. Description of the simplified PBC configuration

The 3D geometry (Fig. 9) corresponds to a PBC setup with $N = 4$ burners similar to Fig. 3 (characteristics defined in Tab. 1). The mean radii R_p and R_c of the cylindrical chamber and plenum are derived from the half perimeter L_p and L_c of the analytical model. Boundary conditions correspond to impermeable walls everywhere.

4.2. Description of the 3D acoustic code

To validate the assumptions used in ATACAMAC formulation, it is interesting to compare its results to the output of a full 3D acoustic solver. Here, AVSP was used: AVSP is a parallel 3D code devoted to the resolution of acoustic modes of industrial combustion chambers [38]. It solves the eigenvalues problem issued from a discretization on unstructured meshes of the Helmholtz equation with a source term due to the flames. The mesh used here (Fig. 9, left) is composed of 230,000 cells which ensures grid independence. The flame-acoustic interaction is taken into account via the FTF model [37] similar to the expression used in Eq. (13). The local reaction term is expressed in burner i as:

$$\dot{w}_i = n_{u,i} e^{j\omega\tau_i} w'(\mathbf{x}_{ref,i}) \quad (41)$$

The local interaction index $n_{u,i}$ describes the local flame-acoustic interactions. The values of $n_{u,i}$ are assumed to be constant in the flame zone i

Chamber			
Half perimeter	L_c	6.59	m
Section	S_c	0.6	m^2
Plenum			
Half perimeter	L_p	6.59	m
Section	S_p	0.6	m^2
Burner			
Length	L_i^0	0.6	m
Section	S_i	0.03	m^2
Fresh gases			
Mean pressure	p^0	$2 \cdot 10^6$	Pa
Mean temperature	T_u^0	700	K
Mean density	ρ_u^0	9.79	kg/m^3
Mean sound speed	c_u^0	743	m/s
Burnt gases			
Mean pressure	p^0	$2 \cdot 10^6$	Pa
Mean temperature	T^0	1800	K
Mean density	ρ^0	3.81	kg/m^3
Mean sound speed	c^0	1191	m/s
Flame parameters			
Interaction index	n_i	<i>variable</i>	–
Time-delay	τ_i	<i>variable</i>	s
Thickness	e_{fl}	0.03	m

Table 1: Parameters used for numerical applications. They correspond to a typical large scale industrial gas turbine.

(Fig. 9) and are chosen to recover the global value of interaction index n_i of the infinitely thin flame when integrated over the flame zone i [38]. They are also assumed to be independent on frequency for simplicity. Heat release fluctuations in each flame zone are driven by the velocity fluctuations at the reference points $\mathbf{x}_{\text{ref},i}$ located in the corresponding burner. In the infinitely thin flame model these reference points are the same as the flame locations z_f . In AVSP, the reference points were placed a few millimeters upstream of the flames (Fig. 9) in order to avoid numerical issues. This was proved to have only a marginal effect on the computed frequency [38, 39].

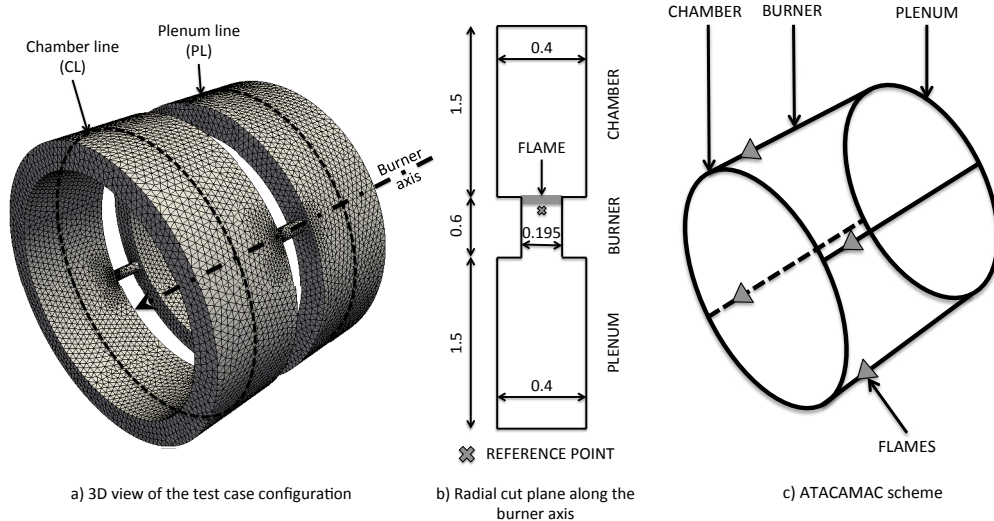


Figure 9: 3D toy-model to validate the ATACAMAC methodology. Perfect annular chamber and plenum connected by four burners ($N = 4$). --- : line in the plenum (PL) and in the chamber (CL) along which absolute pressure and phase will be plotted

4.3. Construction of a quasi-1D network from a real 3D combustor

A quasi-one-dimensional model of a simplified PBC configuration described in Section 4.1 can be constructed using Tab. 1. Even though the present model is quasi-one-dimensional, simple corrections can be incorporated to capture 3D effects.

First, the burners considered in Fig. 9 are long narrow tubes for which end effects modify acoustic modes. In the low frequency range, this can be accounted for [40] and a standard length correction for a flanged tube [41] is applied at the two burner's ends. The corrected length L_i for the burners is:

$$L_i = L_i^0 + 2 \times 0.4 \sqrt{4S_i/\pi} \quad (42)$$

where L_i^0 is the i^{th} burner length without correction and S_i is the surface of the i^{th} burner.

Second, the position of the compact flames is defined via the parameter $\alpha = z_{f,i}/L_i$ where L_i is the corrected burner length and $z_{f,i}$ is the position of the center of the flame. In Sections 5 and 6, the flame position parameter is set to $\alpha = 0.88$, a location chosen because it is far away from all pressure nodes.

5. Mode analysis of a weakly coupled PBC configuration with four burners ($N = 4$)

Under the weak coupling factors assumption ($0 < \wp_{p,i} \ll 1$ and $0 < \wp_{c,i} \ll 1$) frequencies of the whole system can be analyzed considering small perturbations around the chamber alone (FDCp mode at $k^0 L_c = p\pi$) or plenum alone (FDPp mode at $k_u^0 L_p = p\pi$) wave numbers leading to two families of modes which appear separately (Section 3.3):

$$kL_c = p\pi + \epsilon_c \text{ (WCCp)} \quad (43)$$

or

$$k_u L_p = p\pi + \epsilon_p \text{ (WCPp)} \quad (44)$$

where p is the mode order, $\epsilon_c \ll p\pi$ and $\epsilon_p \ll p\pi$. Since the two families of modes behave in the same manner (only radius, density and sound speed are changed), only weakly coupled chamber modes will be detailed in this Section.

Due to symmetry considerations of the case $N = 4$, odd-order modes ($p = 2q + 1$, $q \in \mathbb{N}$) and even-order modes ($p = 2q$, $q \in \mathbb{N}$) will not behave in the same manner and are analyzed in Section 5.1 and 5.2 respectively.

5.1. Odd-order weakly coupled modes of the PBC configuration with four burners ($N = 4$)

Considering odd order modes ($p = 2q + 1$, $q \in \mathbb{N}$) with the low coupling limit assumption ($0 < \wp_{p,i} \ll 1$ and $0 < \wp_{c,i} \ll 1$) leads to the expansion $kL_c = p\pi + \epsilon_c$ (for a WCCp mode). A Taylor expansion can therefore be used to obtain a simplified analytical expression of the transfer matrix of the i^{th} sector and consequently of the dispersion relation (Eq. (25)). This approach is fully detailed in Appendix A for the first mode on a single burner case ($N = 1$) for simplicity. The same approach for the p^{th} mode and four burners ($N = 4$) leads to (see Tab. A.2):

$$\sin(p\pi\beta)^2[\epsilon_c^2 + 4\epsilon_c\Gamma_4^0 + 4\Gamma_4^{02}] + o(\epsilon_c^2) = 0 \quad (45)$$

where $\beta = \frac{c^0 L_p}{c_u^0 L_c}$ and Γ_4^0 is the value of Γ_4 when $kL_c = p\pi$. Note that all the burners share the same length and cross section in this configuration so that the index i of Eq. (20) was removed for simplicity.

The β parameter can be viewed as a tuning parameter between cavities: it compares the period of the azimuthal modes in the plenum alone ($\tau_p^0 = \frac{2L_p}{pc_u^0}$)

and in the chamber alone ($\tau_c^0 = \frac{2L_c}{pc^0}$). In general, the two annular volumes are not tuned and the periods τ_p^0 and τ_c^0 of the azimuthal modes of the plenum and the chamber do not match, i.e. $\beta = \tau_p^0/\tau_c^0 \neq l$, $l \in \mathbb{N}$ (for example for the first chamber and plenum modes ($p = 1$) of Table 1 where $\beta \simeq 1.60$) so that the only solution to satisfy Eq. (45) is:

$$\epsilon_c^2 + 4\epsilon_c\Gamma_4^0 + 4\Gamma_4^{02} + o(\epsilon_c^2) = 0 \quad (46)$$

This quadratic equation has a double root ³ :

$$\epsilon_c = -2\Gamma_4^0 \quad (47)$$

where Γ_4^0 is the value of Γ_4 (Eq. (20)) at $\omega = \omega^0 = p\pi c^0/L_c$

Real and imaginary parts of the frequency obtained in Eq. (47) are compared to the exact numerical resolution of the dispersion relation Eq. (25) and to AVSP results in Fig. 10. A very good agreement is found showing that the asymptotic expression of Eq. (47) is correct.

From Eq. (47), a simple analytical stability criterion can be derived as explained in Appendix B for weakly coupled chamber modes (Eq. (B.3)):

$$\underbrace{\sin\left(2\pi\frac{\tau}{\tau_c^0}\right)}_{\text{effect of } \tau} \underbrace{\sin\left(2p\pi\frac{\alpha L_i c^0}{L_c c_u^0}\right)}_{\text{effect of } \alpha} < 0 \quad (\text{WCCp modes}) \quad (48)$$

where $\tau_c^0 = \frac{2c^0}{pL_c}$

Time-delay τ of the FTF and flame position α have an effect on the stability and can be studied separately:

- **Time-delay** - From Eq. (48), a critical time-delay controlling the transition from stable to unstable regimes can be obtained: $\tau_{crit} = \tau_c^0/2 = \frac{L_c}{pc^0}$ for WCCp modes. This result being also valid for plenum modes (i.e. WCPp modes, see Eq. (B.4) leading to the critical time-delay

³This approach can be extended at higher orders to unveil plenum/chamber interactions. From a third-order truncation of the dispersion relation (Eq. 25), a second-order correction on eigenfrequencies found in Eq. (47) is obtained for WCCp modes:

$$\epsilon_c = -2\Gamma_4^0 - H(\beta)\Gamma_2^0\Gamma_3^0 \quad (\text{WCCp modes})$$

where $H(\beta) = 4 \tan(p\pi\beta/2)$.

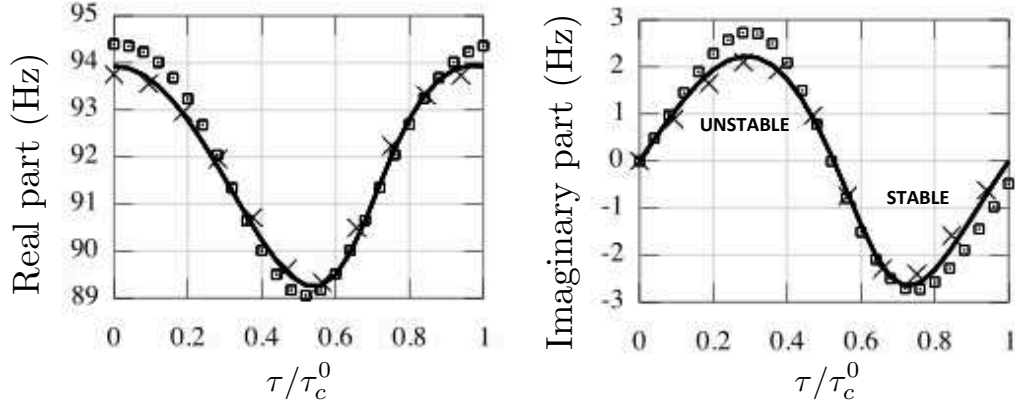


Figure 10: Eigenfrequency of the WCC1 mode for four burners ($N = 4$) with $n_i = 1.57$ as a function of τ/τ_c^0 . — : Numerical resolution of the dispersion relation Eq. (25), \square : Analytical model prediction Eq. (47), \times : AVSP results

$\tau_p^0/2 = \frac{L_p}{pc_u^0}$), stability ranges of the two first azimuthal modes WCC1 and WCP1 can be displayed simultaneously (Fig. 11). It shows that the region where both the chamber and plenum modes are stable is smaller than the stability ranges of modes taken separately: stabilizing one mode of the system cannot ensure the stability of the whole system. Of course, this result does not include any dissipation or acoustic fluxes through the boundaries [42] which would increase stability regions.

- **Flame position** - Similarly to longitudinal modes in the Rijke tube [26, 2, 43], the flame position (defined by α) also controls the stability (Eq. (48)). Appendix C demonstrates an analytical expression of the critical flame position for weakly couple modes (Eq. (C.2)) at which the stability change occurs. These expressions are close to the solution found in Rijke tubes (Eq. (C.1)) and have been validated for several weakly coupled modes (Tab. C.4 and Fig. C.22).

5.2. Even-order modes of the PBC configuration with four burners ($N = 4$)

Considering even-order weakly coupled chamber modes ($p = 2q$, $q \in \mathbb{N}$) and using Eq. (25) with the low coupling limit assumption ($0 < \wp_{p,i} \ll 1$ and $0 < \wp_{c,i} \ll 1$), the dispersion relation (Eq. (25)) becomes (Tab. A.2):

$$\sin(p\pi\beta/2)^2[\epsilon_c^2 + 4\epsilon_c\Gamma_4^0] + o(\epsilon_c^2) = 0 \quad (49)$$

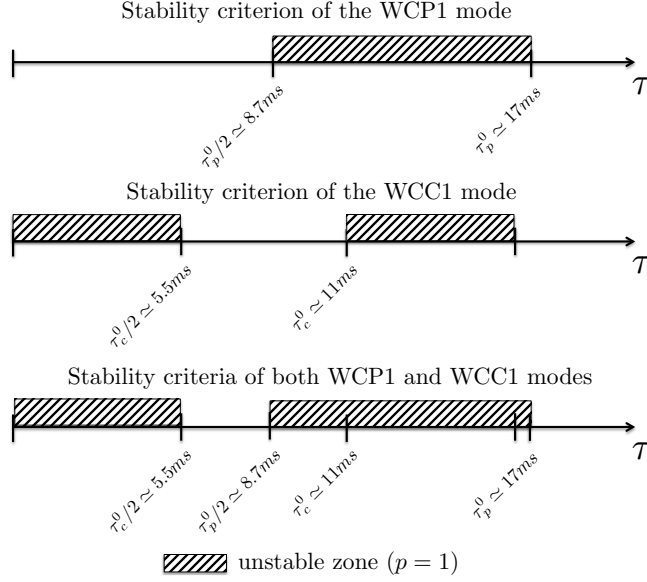


Figure 11: Stability maps (Eq. (48)) of the two first azimuthal modes ($p = 1$) for a flame located at $\alpha \simeq 0.88$: WCP1 (top), WCC1 (middle) and both WCP1 and WCC1 (bottom)

where $\beta = \frac{k_u L_p}{k L_c}$ and Γ_4^0 is the value of Γ_4 when $k L_c = p\pi$.

When chamber and plenum frequencies do not match, i.e. $\beta \neq 1$ (for example for the second ($p = 2$) mode of Table 1 where $\beta \simeq 1.60$), the only solution to satisfy Eq. (49) is to have:

$$\epsilon_c^2 + 4\epsilon_c \Gamma_4^0 + o(\epsilon_c^2) = 0 \quad (50)$$

This quadratic equation has two distinct roots:

$$\epsilon_c = 0 \text{ and } \epsilon_c = -4\Gamma_4^0 \quad (51)$$

The first solution ($\epsilon_c = 0$) of Eq. (51) corresponds to modes which are not affected by the flames: the symmetry of the four burners case ($N = 4$) allows even-order modes to impose a pressure node at each burner location suppressing the flame effect on these modes which become neutral.

The second solution of Eq. (51) ($\epsilon_c = -4\Gamma_4^0$) correspond to modes which are modes strongly affected by the flame because it imposes a pressure anti-node (maximum pressure) downstream of each burner.

Real and imaginary parts of the frequency obtained from Eq. (51) are compared to the numerical solutions of the dispersion relation Eq. (25) and

to AVSP results in Fig. 12. A very good agreement is found and the non-perturbed mode ($\epsilon_c = 0$) is correctly captured (straight lines).

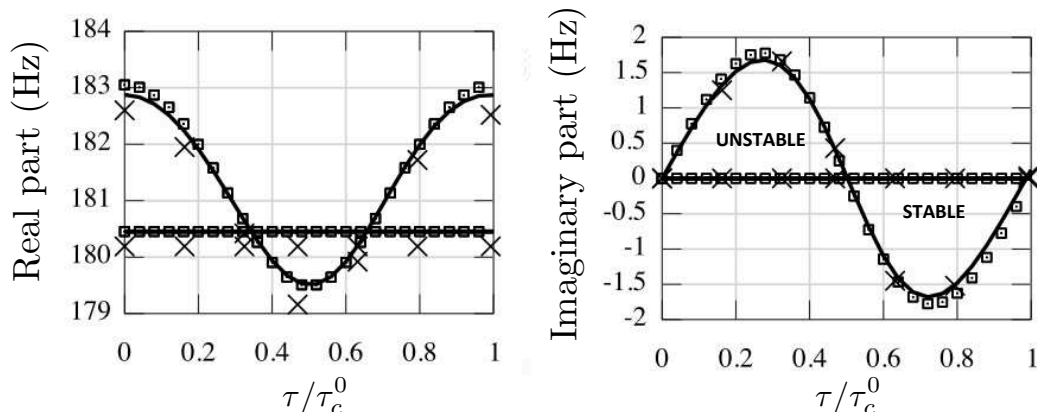


Figure 12: Eigenfrequency of the WCC2 mode for four burners ($N = 4$) with $n_i = 1.57$ as a function of τ/τ_c^0 . — : Numerical resolution of the dispersion relation Eq. (25), \square : Analytical model prediction Eq. (51), \times : AVSP results

Using Eq. (51) and Appendix B leads to an analytical stability criterion for WCCp even-order modes (Eq. (B.3)). This result being also valid for WCPp modes (Eq. (B.4)) and using the results from Section 5.1, stability maps of the weakly coupled plenum and chamber modes (WCC1, WCC2, WCP1 and WCP2) can be plotted together (Fig. 13) highlighting the difficulty to get a stable system in the absence of dissipation as supposed here: considering only these four modes, no stable region is found for time-delays lower than $19.1ms$ in the case described in Tab. 1 (Fig. 13).

5.3. Mode structure of weakly coupled modes

In weakly coupled situations, acoustic activity is present only in one annular cavity and in the burners as shown in Fig. 14 for the WCC1 mode (the same mode with the opposite rotation direction is also captured by AVSP but not shown here). Fig. 15 shows that this mode is purely rotating in the chamber while it is mixed in the plenum. Therefore, the combination of the two weakly coupled chamber modes with the clockwise rotation (show in Fig. 15) and the anti-clockwise rotation (not shown) enable to have purely rotating or purely standing modes but not necessarily in the two annular cavities at the same time.

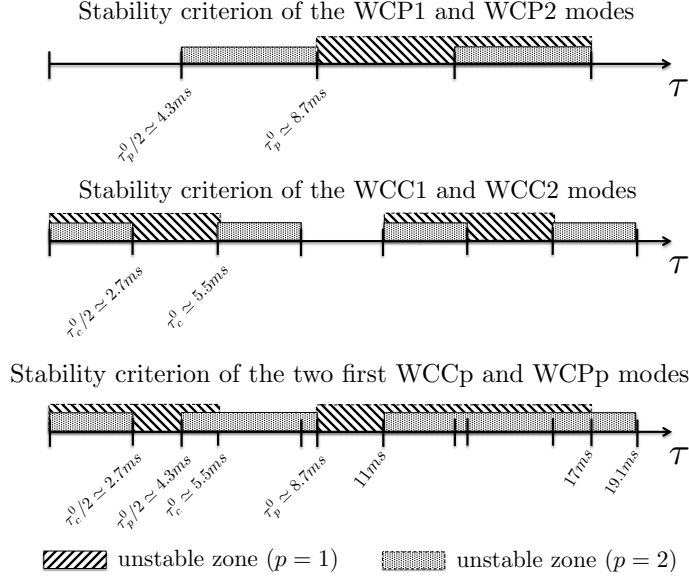


Figure 13: Stability maps of the WCC1, WCC2, WCP1 and WCP2 modes

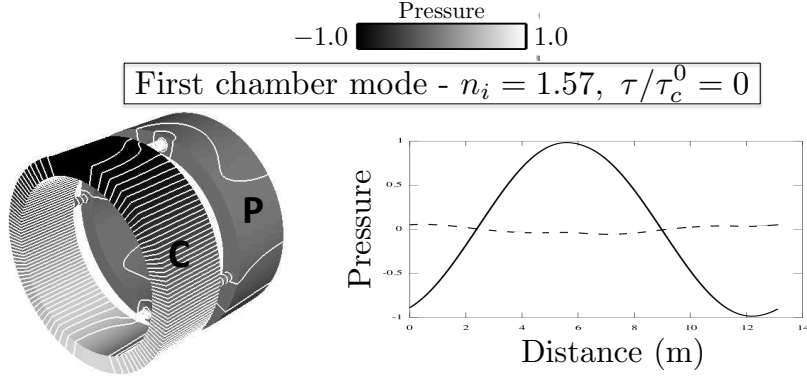


Figure 14: Pressure mode structures ($p' = |p'| \cos(\arg(p'))$) obtained with AVSP with pressure isolines (left) and pressure along the azimuthal direction in the annular chamber (—) and annular plenum (---) for the WCC1 mode of a PBC configuration with four burners ($N = 4$) and $n_i = 1.57$ at the time-delay: $\tau/\tau_c^0 = 0$

5.4. Stability map of weakly coupled situations

Sections 5.1 and 5.2 focused on weakly coupled situations where the low coupling factor assumption ($\varphi_p \ll 1$ and $\varphi_c \ll 1$) is valid. Stability maps of perturbed modes (i.e. $\epsilon \neq 0$) in the complex plane $[R_e(f), I_m(f)]$ are well

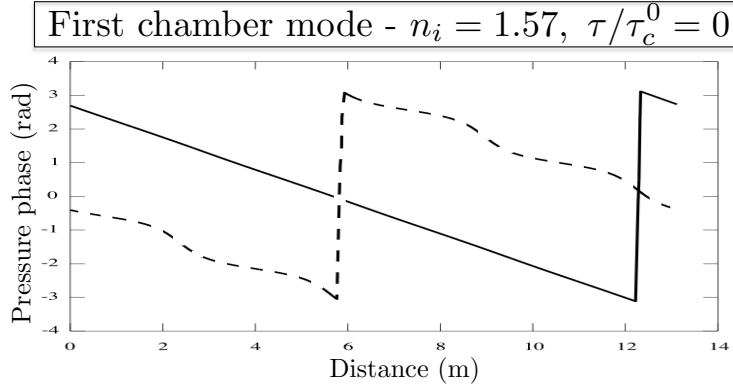


Figure 15: Pressure phase of the WCC1 mode obtained with AVSP at $n_i = 1.57$ along the azimuthal direction in the annular chamber (—) and the annular plenum (---) for time-delay: $\tau/\tau_c^0 = 0$

suites to show differences between the several regimes - weakly coupled and strongly coupled situations. These maps are oriented circles (--- (WCP1) and — (WCC1) in Fig.16) centered at the frequency $f(n_i = 0) \simeq f_0$ which corresponds to a passive flame mode ($n_i = 0$: \times in Fig.16) and is approximately the frequency of the cavity alone ($f_0 = \frac{pc^0}{2L}$). The radius is proportional to the coupling factor which can be increased via the surface ratios (S_i/S_p and S_i/S_c) or the flame interaction index n_i . In the weakly coupled regime, WCCp and WCPp modes do not strongly interact as shown in Fig. 16: modes in the plenum and in the chamber live separately.

6. Mode analysis of a strongly coupled PBC configuration with four burners ($N = 4$)

For weakly coupled cases (Section 5), the frequencies of the azimuthal modes in the plenum and in the chamber are only marginally affected by the flame (Figs. 10 and 12) so that they can never match (Fig. 16). However, if the flame interaction index (n_i) is larger, the frequencies of the azimuthal modes of the annular plenum and the annular chamber change more and the possibility of having these two frequencies match opens an interesting situation where the whole system can resonate. This corresponds to the strongly coupled modes of order p (referred as "SCp" modes) studied in this section.

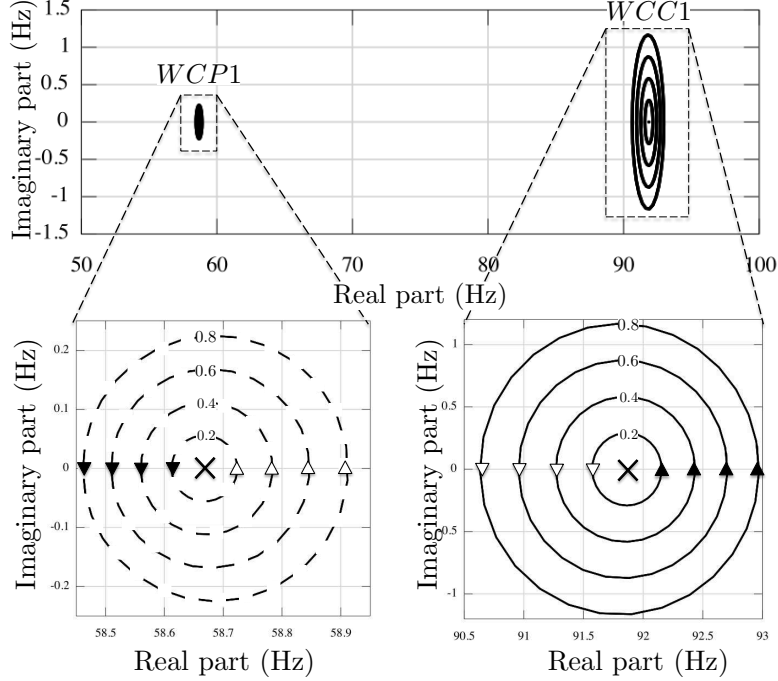


Figure 16: Eigenfrequencies of both WCP1 and WCC1 modes (top) and zoom on WCP1 (bottom left) and WCC1 (bottom right) when the flame delay changes for PBC configuration with four burners ($N = 4$) with $n_i = 0.2, 0.4, 0.6$ and 0.8 , \times : Passive flame ($n_i = 0$), $---$: WCP1 mode, $---$: WCC1 mode, \blacktriangleright : $\tau/\tau_p^0 = 0$ or $\tau/\tau_c^0 = 0$ oriented in the increasing τ direction, \triangleright : $\tau/\tau_p^0 = 1/2$ or $\tau/\tau_c^0 = 1/2$

Figure 17 shows the stability maps of the WCC1 ($---$) and WCP1 ($---$) modes obtained with low flame interaction index ($n_i = 5.0$ and 6.0) as well as the SC1 (\circ) and SC2 modes (\bullet) obtained for higher flame interaction index ($n_i = 7.0$ and 8.0^4 at the zero frequency limit). Three points in the SC2 trajectory with $n_i = 8.0$ corresponding to several time-delays ($\tau/\tau_c^0 = 0$ (A), $\tau/\tau_c^0 = 0.54$ (B) and $\tau/\tau_c^0 = 0.9$ (C)) are displayed in Fig. 17 and will be used as typical cases to show pressure structures in the annular plenum and chamber.

For low flame interaction index ($n_i = 5.0$ and 6.0), the first two modes always have different frequencies and can be identified as plenum (WCPp:

⁴Note that the typical order of magnitude of the interaction index n_i is $T_b/T_u - 1$

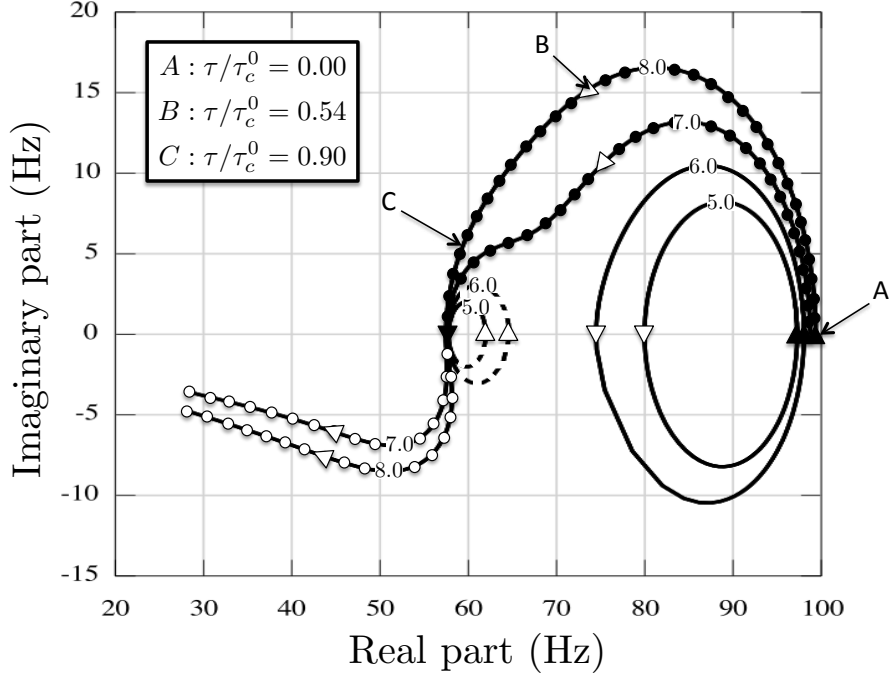


Figure 17: Eigenfrequencies on the complex plane for a PBC configuration with four burners ($N = 4$), --- : WCP1 mode ($n_i = 5.0$ and 6.0), — : WCC1 mode ($n_i = 5.0$ and 6.0), \circ : SC1 mode ($n_i = 7.0$ and 8.0), \bullet : SC2 mode ($n_i = 7.0$ and 8.0), \blacktriangleright : $\tau/\tau_p^0 = 0$ oriented in the increasing τ direction and \triangleright : $\tau/\tau_p^0 = 1/2$ or $\tau/\tau_c^0 = 1/2$

---) or chamber modes (WCCp: —) as studied in Section 5.

However, for higher flame interaction indices ($n_i = 7.0$ and 8.0) a bifurcation occurs: frequencies of the annular plenum, burners and annular chamber can match leading to strongly coupled modes where the whole system resonates. The trajectory of the first strongly coupled mode (SC1: \circ) goes from the WCP1 mode (for small time-delays $\tau < \tau_p^0/2$) to a longitudinal mode (not presented here around 40Hz, for large time-delays $\tau > \tau_p^0/2$). A second strongly coupled mode (SC2: \bullet) has a trajectory in the complex plane coming from the WCC1 mode (for small time-delays $\tau < \tau_c^0/2$) and going to the WCP1 mode (for large time-delays $\tau > \tau_c^0/2$).

The stability map of the SC2 mode (\bullet) at $n_i = 8.0$ has been validated against the 3D finite element solver AVSP (Fig. 18). A good agreement between AVSP (\times) and the numerical resolution of Eq. (25) (—) is found. The growth rate is slightly underestimated but the global trend is well cap-

tured: the mode is fully unstable for all time-delays which corresponds to a new behavior compared to the weakly coupled modes. The analytical approach developed in Section 5 for the weakly coupled regime (\square in Fig. 18) is not able to capture this new highly non-linear behavior.

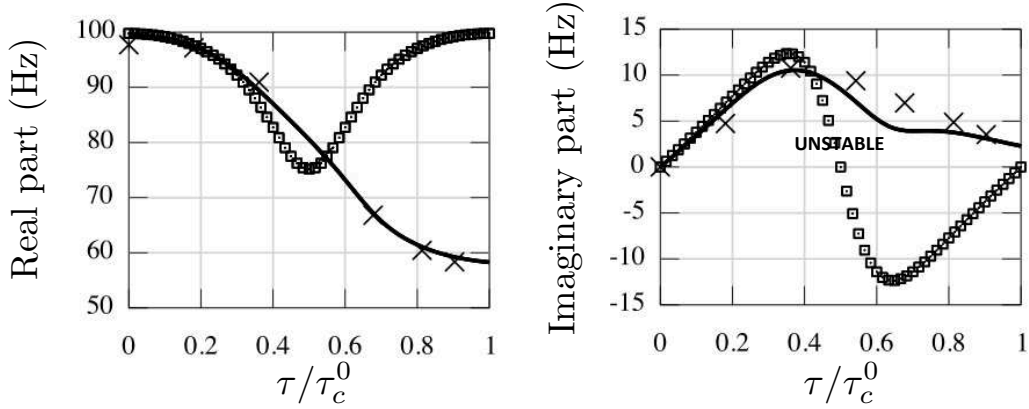


Figure 18: Eigenfrequency of the first order chamber mode ($p = 1$) for four burners ($N = 4$) as a function of τ/τ_c^0 with $n_i = 8.0$. — : Numerical resolution of Eq. (25), \square : Analytical model prediction for weakly coupled situations (Eq. (47)), \times : AVSP results

When the flame interaction index is sufficiently large ($n_i > 7.0$), i.e. when the flame is sufficiently intense, the modes of plenum and chamber lock-in and become unstable for all time delays. Fig. 19 shows the modulus of the coupling factors $\|\Gamma_1\|$, $\|\Gamma_4\|$ and the interaction product $\|\Gamma_2\Gamma_3\|$ (terms appearing in analytical results summarized in Tab. B.3) as a function of the time-delay τ_1 for the three different cases corresponding to the first order ($p = 1$) chamber mode: $n_1 = 1.57$ (weakly coupled regime), $n_1 = 4.0$ (limit case between weakly/strongly coupled regimes) and $n_1 = 8.0$ (strongly coupled regime). It highlights the tuning mechanism:

- In the weakly coupled regime ($n_1 = 1.57$), both Γ_1 and Γ_4 have the same order of magnitude and they vary in opposite directions. The low coupling factors assumption is satisfied.
- Then, at the limit case between weakly/strongly coupled regime ($n_1 = 4.0$), $\|\Gamma_4\|$ is almost constant with the time-delay τ_1 . The other coupling factors are not affected.
- Finally, in the strongly coupled regime ($n_1 = 8.0$), the coupling parameter of the burner/chamber junction Γ_4 is amplified which indicates

that this junction is tuned. The evolution with the time-delay is reversed compared to the weakly coupled regime: now, the two annular cavities (plenum and chamber) act together in the same manner ; they are coupled. Consequently, the interaction term ($\|\Gamma_2\Gamma_3\|$) is also increased. The low coupling factors assumption is not satisfied in this case.

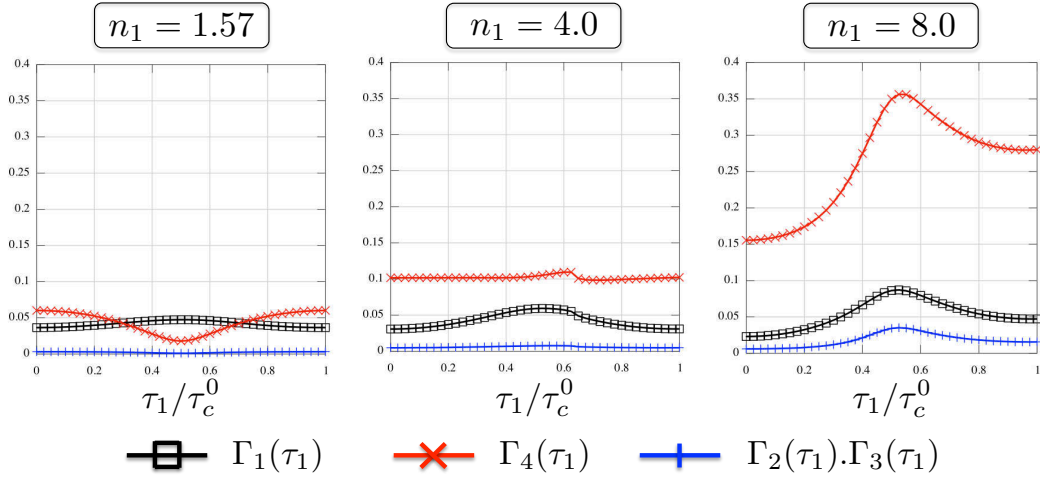


Figure 19: Modulus of the coupling factors $\|\Gamma_1\|$ (\square), $\|\Gamma_4\|$ (\times) and $\|\Gamma_2 * \Gamma_3\|$ ($+$) varying with the time delay τ_1 for three cases: $n_1 = 1.57$ (weakly coupled regime), $n_1 = 4.0$ (limit case) and $n_1 = 8.0$ (strongly coupled regime)

Pressure structures ($p' = |p'| \cos(\arg(p'))$) along the azimuthal direction in the plenum (PL line in Fig. 9) and in the chamber (CL line in Fig. 9) obtained with AVSP for the second strongly coupled mode are displayed in Fig. 20 for a high flame interaction index ($n_i = 8.0$) and several time-delays (A: $\tau/\tau_c^0 = 0$, B: $\tau/\tau_c^0 = 0.54$ and C: $\tau/\tau_c^0 = 0.9$ from Fig. 17). For null time-delays (A in Fig. 17), acoustic activity is only present in the chamber (—) and the frequency is close to the weakly coupled chamber mode. The acoustic activity in the second annular cavity (i.e. the plenum: ---) grows with the time-delay τ . For $\tau/\tau_c^0 = 0.54$ ms (B in Fig. 17) a strong interaction with the burners appears leading to higher growth rates. Surprisingly, this case corresponds only to a moderate acoustic activity in the second annular cavity (i.e. the annular plenum: ---). For $\tau/\tau_c^0 = 0.9$ (C in Fig. 17) a first order mode is present in both annular cavities highlighting a strongly coupled

situation. This strong interaction between plenum and chamber revealed by the presence of acoustic activity in both annular cavities leads, however, to a marginally unstable mode.

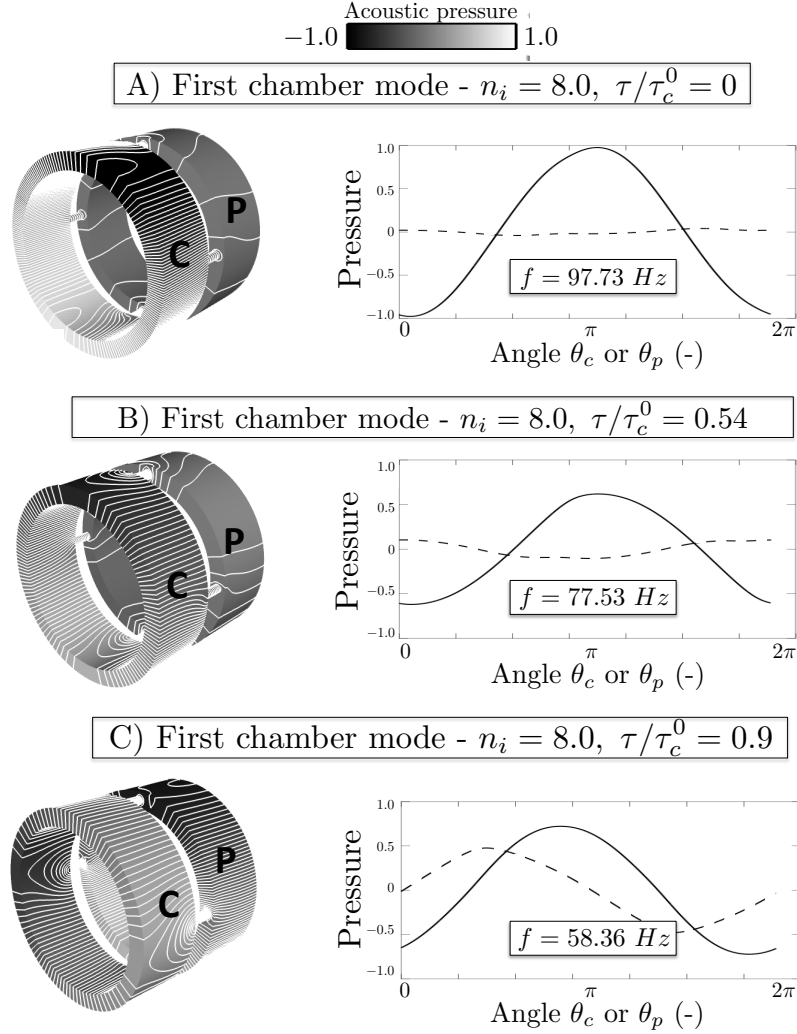


Figure 20: Pressure structures and isolines ($p' = |p'| \cos(\arg(p'))$) obtained with AVSP (left) and pressure along the azimuthal direction in the annular chamber (—) and annular plenum (---) for the SC2 mode of a PBC configuration with four burners ($N = 4$) and $n_i = 8.0$ at several time-delay: $\tau/\tau_c^0 = 0$ (top), 0.54 (middle) and 0.9 (bottom). The configuration corresponds to $f_{FDP1} = 56$ Hz and $f_{FDC1} = 90$ Hz

Fig. 21 shows the pressure phase in the annular plenum (---) and in the

annular chamber (—) for several time-delays. The same mode with opposite direction is also found with AVSP but not shown here. For small time-delay ($\tau/\tau_c^0 = 0$ for case A and $\tau/\tau_c^0 = 0.54$ for case B of Fig. 17), pressures in the plenum and in the chamber have different natures: purely spinning mode in the chamber (linear phase) and a mixed mode in the plenum (wave shape of the phase). The combination of clockwise and anti-clockwise mode can generate purely spinning or purely standing mode but not necessarily in both annular cavities at the same time. However, higher time-delays cases (as for case C where $\tau/\tau_c^0 = 0.9$) correspond to strongly coupled situations where both annular cavities lock-in (Fig. 20 C). In such a case, pressure in the chamber and plenum exhibit the same nature: purely spinning in both cavities in Fig. 21 C (the same mode with the opposite rotating direction is also found by AVSP but not shown here). The combination of the purely spinning modes (clockwise and anti-clockwise) can also lead to standing modes in both annular cavities at the same time: this is a specific behavior only encountered in locked-in modes as case C.

Finally, it demonstrates that a highly unstable mode does not necessarily exhibit strong acoustic activity in both annular cavities (as for case B) and that a mode where acoustic activity appears in the whole system can be only marginally unstable (as for case C). Moreover, the phase-lag between pressure in the annular cavity and the annular chamber as well as the nature of the mode (spinning, standing or mixed) changes when acoustic activity is present in both annular cavities, a property which could be checked experimentally.

7. Conclusion

To complement expensive Large Eddy Simulation [44] and Helmholtz [38] 3D codes used to study azimuthal modes in annular combustors, simple tools are required to understand the physics of these modes and create pre-designs of industrial combustors. This paper describes a simple analytical theory to compute the azimuthal modes appearing in these combustors. It is based on a quasi-one-dimensional acoustic network where N burners are connected to an annular plenum and chamber. A manipulation of the corresponding acoustic equations in this configuration leads to a simple analytical dispersion relation which can be solved numerically. This method allows to exhibit coupling factors between plenum, burners and chamber which depend on area ratios and flame transfer function (FTF). For $N = 4$, a fully analytical resolution can be performed in specific situations where coupling factors of the FTF [22, 26]

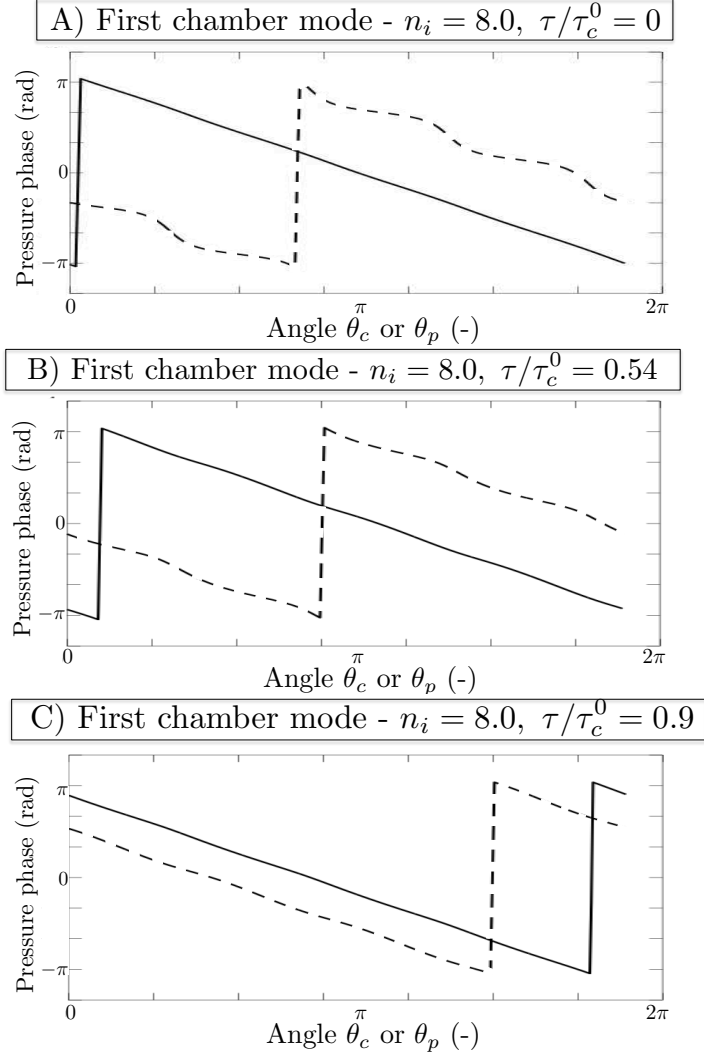


Figure 21: Pressure phase obtained with AVSP for the SC2 mode at $n_i = 8.0$ along the azimuthal direction in the annular chamber (—) and the annular plenum (---) for several time-delays: $\tau/\tau_c^0 = 0$ (top), 0.54 (middle) and 0.9 (bottom).

are small and simple stability criteria can be proposed. For higher coupling factors, a bifurcation occurs yielding a strongly coupled regime where acoustic activity is present in both annular cavities. The nature of such a mode (standing, spinning or mixed) changes with the time-delay. Purely spinning or purely standing modes in the annular plenum and in the chamber were

compute analytically the determinant leading to the exact dispersion relation:

$$\begin{aligned}
& (\Gamma_1\Gamma_4 - \Gamma_2\Gamma_3) \sin(2kL_c) \sin(2k_uL_p) \\
& + 2\Gamma_1[1 - \cos(2kL_c)] \sin(2k_uL_p) \\
& + 2\Gamma_4[1 - \cos(2k_uL_p)] \sin(2kL_c) \\
& + 4[1 - \cos(2kL_c)][1 - \cos(2k_uL_p)] = 0
\end{aligned} \tag{A.2}$$

The dispersion relation Eq. (A.2) is non-linear. The idea is to use a Taylor expansion at the second (or third) order and to solve it analytically. The expansion has to be done around a FDCp (i.e. $kL_c = p\pi + \epsilon_c$) or FDPp (i.e. $k_uL_p = p\pi + \epsilon_p$) mode (see Section 3.3 for details). For instance, in the case of the WCC1 mode ($kL_c = \pi + \epsilon$ which implies $k_uL_p = \beta(\pi + \epsilon_c)$ where $\beta = \frac{c^0L_p}{c_u^0L_c}$), the dispersion relation Eq. (A.2) becomes:

$$[\cos(2\pi\beta) - 1][\epsilon_c\Gamma_4^0 + \epsilon_c^2 + o(\epsilon_c^2)] = 0 \tag{A.3}$$

where Γ_4^0 is the value of Γ_4 evaluated at $kL_c = p\pi$

Note that solutions of Eq. (A.3) being $\epsilon_c = -\Gamma_4^0$, it justifies that the term $\epsilon_c\Gamma_4^0$ is of the same order of magnitude than ϵ_c^2 and therefore has to be kept in the analytical dispersion relation Eq. A.2.

Analytical dispersion relations for $N > 1$ are more complex to derive but follow a similar procedure. When $N = 4$, the dispersion relation of Tab. (A.2) are obtained:

Type	Odd/Even	Second-order dispersion relation ($o(\epsilon^2)$)
WCC	Odd	$\sin(p\pi\beta)[\epsilon^2 + 4\epsilon\Gamma_4^0 + 4\Gamma_4^{02}] = 0$
	Even	$\sin(p\pi\beta/2)[\epsilon^2 + 4\epsilon\Gamma_4^0] = 0$
WCP	Odd	$\sin(p\pi/\beta)[\epsilon^2 + 4\epsilon\Gamma_1^0 + 4\Gamma_1^{02}] = 0$
	Even	$\sin(p\pi/(2\beta))[\epsilon^2 + 4\epsilon\Gamma_1^0] = 0$

Table A.2: Analytical expressions of wave number perturbation for WCCp and WCPp azimuthal modes

Appendix B. Stability criterion of weakly coupled modes for a four burners configuration ($N = 4$)

A mode is stable if the imaginary part of the wave number is negative. Table B.3 shows analytical expressions of the wave number perturbation ϵ for WCPp and WCCp modes⁶:

Type	Odd/Even	Wave number perturbation (ϵ)
WCC	Odd	$-2\Gamma_4^0 - H(\beta)\Gamma_2^0\Gamma_3^0$
	Even	$-2\Gamma_4^0 - G(\beta)\Gamma_2^0\Gamma_3^0$
WCP	Odd	$-2\Gamma_1^0 - H(1/\beta)\Gamma_2^0\Gamma_3^0$
	Even	$-2\Gamma_1^0 - G(1/\beta)\Gamma_2^0\Gamma_3^0$

Table B.3: Analytical expressions of wave number perturbation ϵ for WCCp and WCPp modes where $H(x) = 4 \tan(p\pi x/2)$ and $G(x) = 4 \frac{\sin(p\pi x/2)}{\cos(p\pi x/2) - (-1)^{p/2}}$ have real values.

Analytical stability criteria can be derived by calculating the sign of $Im(\Gamma_1^0)$, $Im(\Gamma_4^0)$ and $Im(\Gamma_2^0\Gamma_3^0)$ using the following definitions: \mathbb{F}^* is the complex conjugate of the flame parameter $\mathbb{F} = \frac{\rho^0 c^0}{\rho_u^0 c_u^0} (1 + n.e^{j\omega^0\tau})$, $\theta^0 = \omega^0(1 - \alpha)L_i/c^0 \in \mathbb{R}$ and $\theta_u^0 = \omega^0\alpha L_i/c_u^0 \in \mathbb{R}$. The notation \mathfrak{D} refers to $\mathfrak{D} = |\cos(\theta^0) \sin(\theta_u^0) + \mathbb{F} \sin(\theta^0) \cos(\theta_u^0)|^2$

With these notations, the sign of the imaginary part of these coupling parameters are:

$$Im(\Gamma_1^0) = \frac{S_i}{4S_p\mathfrak{D}} \sin(2\theta^0)Im(\mathbb{F}) \quad (\text{B.1})$$

$$Im(\Gamma_4^0) = -\frac{S_i}{4S_c\mathfrak{D}} \sin(2\theta_u^0)Im(\mathbb{F}) \quad (\text{B.2})$$

Eqs. (B.1 - B.2) lead to simple analytical stability criteria for WCCp and

⁶Since all sectors are identical, the index i has been omitted to simplify notations (e.g Γ_1 instead of $\Gamma_{i,1}$)

WCCp modes:

$$\sin(2p\tau/\tau_c^0) \sin\left(2p\pi\frac{\alpha L_i c_u^0}{L_c c_u^0}\right) < 0 \text{ for WCCp modes} \quad (\text{B.3})$$

$$\sin(2p\tau/\tau_p^0) \sin\left(2p\pi\frac{(1-\alpha)L_i c_u^0}{L_p c^0}\right) > 0 \text{ for WCCp modes} \quad (\text{B.4})$$

Appendix C. Flame position effect on annular combustors stability

Similarly to longitudinal modes in the Rijke tube [26, 2, 43], the flame position (defined by α) also controls the stability (Eq. (48)). In a quasi-isothermal Rijke tube, for common (small) values of the FTF time-delay τ , stability of the first longitudinal mode is obtained only when the flame is located in the upper half of the tubes [45, 46], i.e. $\alpha > 1/2$, which can be extended for the p -th longitudinal mode:

$$\frac{2m+1}{2p} < \alpha < \frac{2(m+1)}{2p}, \quad \forall m \in \mathbb{N} \text{ (Rijke tube)} \quad (\text{C.1})$$

Eq. (48) highlights a similar behavior for azimuthal modes in a PBC configuration: for a WCCp mode with small values of the time-delay $\tau < \tau_c^0/2$, $\sin(2p\frac{\tau}{\tau_c^0})$ is positive and Eq. (48) leads to:

$$\frac{2m+1}{2p} \frac{L_c c_u^0}{L_i c^0} < \alpha < \frac{2(m+1)}{2p} \frac{L_c c_u^0}{L_i c^0}, \quad \forall m \in \mathbb{N} \text{ (WCCp modes)} \quad (\text{C.2})$$

Usually, the critical flame position $\alpha_{crit} = \frac{L_c c_u^0}{2p L_i c^0}$ is larger than unity because the half-perimeter of the annular cavity is much longer than the burner length ($L_c \gg L_i$). Since the range of the normalized flame position α is $[0-1]$, the flame position may affect the stability only for high-order modes (i.e. p large enough to get $\alpha_{crit} < 1$). For instance, in the case described in Table 1 with the corrected burner length $L_i \simeq 0.76 m$, the critical flame positions α_{crit} and the stability ranges (Eq. (C.2)) are shown in Tab. C.4.

The change of stability with the flame position α for small time-delays predicted in Tab. C.4 has been validated using the numerical resolution of the dispersion relation (Eq. (25)) in Fig. C.22. The critical flame positions obtained in Tab. C.4 are well captured for all modes. A situation where the plenum/chamber interaction is not negligible is shown for the WCC1 mode with $\alpha = 0.3$ (i.e. the flame is close the pressure node imposed by the large annular plenum).

Mode order (p)	$p = 1$	$p = 3$	$p = 5$	$p = 7$
$\alpha_{crit} = \frac{L_c c_u^0}{2pL_i c^0}$	2.70	0.9	0.54	0.39
α satisfying Eq. (C.2)	none	[0.9 - 1]	[0.54 - 1]	[0.39 - 0.78]

Table C.4: Critical flame positions α_{crit} and flame positions satisfying Eq. (C.2) for WCCp odd-order modes of the case described in Table 1

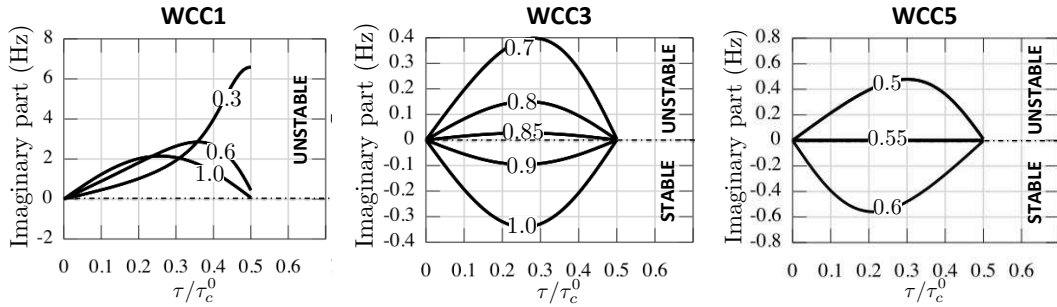


Figure C.22: Growth rate for several flame positions α of the WCC1 ($\alpha = 0.3, 0.6, 1.0$ - left), WCC3 ($\alpha = 0.5, 0.8, 0.85, 0.9, 1.0$ - middle) and WCC5 ($\alpha = 0.5, 0.55, 0.6$ - right) modes for small time delays ($\tau/\tau_c^0 < 1/2$) using the numerical resolution of the dispersion relation (Eq. (25)) with $n_i = 1.57$

References

- [1] W. Krebs, P. Flohr, B. Prade, S. Hoffmann, *Combust. Sci. Tech.* 174 (2002) 99–128.
- [2] T. Poinso, D. Veynante, *Theoretical and Numerical Combustion*, Third Edition (www.cerfacs.fr/elearning), 2011.
- [3] T. Lieuwen, V. Yang, *Combustion Instabilities in Gas Turbine Engines. Operational Experience, Fundamental Mechanisms and Modeling*, volume 210, *Progress in Astronautics and Aeronautics*, AIAA, 2005.
- [4] N. Worth, J. Dawson, *Proceedings of the Combustion Institute* 34 (2013) 3127–3134.
- [5] N. Noiray, M. Bothien, B. Schuermans, *Combust. Theory and Modelling* (2011) 585–606.

- [6] J. Kopitz, A. Huber, T. Sattelmayer, W. Polifke, in: Int'l Gas Turbine and Aeroengine Congress & Exposition, ASME GT2005-68797, Reno, NV, U.S.A.
- [7] S. R. Stow, A. P. Dowling, in: ASME Paper 2003-GT-38168, Atlanta, Georgia, USA.
- [8] S. Evesque, W. Polifke, in: International Gas Turbine and Aeroengine Congress & Exposition, ASME Paper, volume GT-2002-30064.
- [9] S. R. Stow, A. P. Dowling, in: ASME Paper, 2001-GT-0037, New Orleans, Louisiana.
- [10] D. Fanaca, P. Alemela, F. Ettner, C. Hirsch, T. Sattelmayer, B. Schuermans, in: ASME Turbo Expo, GT2008-50781.
- [11] D. Fanaca, P. Alemela, C. Hirsch, T. Sattelmayer, B. Schuermans, Journal of Engineering for Gas Turbines and Power 132 (2010) 071502.
- [12] J.-F. Bourgooin, D. Durox, T. Schuller, J. Beaunier, S. Candel, Combustion and Flame 160 (2013) 1398–1414.
- [13] K. Kunze, C. Hirsch, T. Sattelmayer, in: ASME Turbo Expo, GT2004-53106.
- [14] J. Moeck, M. Paul, C. Paschereit, in: ASME Turbo Expo 2010 GT2010-23577.
- [15] J.-F. Bourgooin, D. Durox, J. Moeck, T. Schuller, S. Candel, in: ASME Turbo Expo, GT2013-95010.
- [16] C. Fureby, Flow, Turb. and Combustion 84 (2010) 543–564.
- [17] P. Wolf, G. Staffelbach, L. Gicquel, J. Muller, T. Poinsot, Combustion and Flame 159 (2012) 3398–3413.
- [18] M. Leyko, F. Nicoud, S. Moreau, T. Poinsot, C. R. Acad. Sci. Mécanique 337 (2009) 415–425.
- [19] C. Sensiau, F. Nicoud, T. Poinsot, Int. Journal Aeroacoustics 8 (2009) 57–68.

- [20] G. Campa, S. Camporeale, A. Guaus, J. Favier, M. Bargiacchi, A. Bottaro, E. Cosatto, G. Mori, GT2011-45969.
- [21] C. Pankiewitz, T. Sattelmayer, ASME Journal of Engineering for Gas Turbines and Power 125 (2003) 677–685.
- [22] J. Parmentier, P. Salas, P. Wolf, G. Staffelbach, F. Nicoud, T. Poinsot, Combustion and Flame 159 (2012) 2374–2387.
- [23] G. Ghirardo, M. Juniper, Proceedings of the Royal Society A 469 (2013).
- [24] S. Evesque, W. Polifke, C. Pankiewitz, in: 9th AIAA/CEAS Aeroacoustics Conference, volume AIAA paper 2003-3182.
- [25] B. Schuermans, C. Paschereit, P. Monkewitz, in: 44th AIAA Aerospace Sciences Meeting and Exhibit, 2006-0549.
- [26] T. Schuller, D. Durox, P. Palies, S. Candel, Combustion and Flame 159 (2012) 1921–1931.
- [27] S. Stow, A. Dowling, in: ASME Turbo Expo, GT2004-54245.
- [28] P. Palies, D. Durox, T. Schuller, S. Candel, Combustion and Flame 158 (2011) 1980–1991.
- [29] P. Huerre, P. Monkewitz, Annual review of fluid mechanics 22 (1990) 473–537.
- [30] F. E. Marble, S. Candel, J. Sound Vib. 55 (1977) 225–243.
- [31] G. Staffelbach, L. Gicquel, G. Boudier, T. Poinsot, Proc. Combust. Inst. 32 (2009) 2909–2916.
- [32] J. O’Connor, T. Lieuwen, Physics of fluids 24 - 075107 (2012).
- [33] J. O’Connor, T. Lieuwen, Journal of Engineering for Gas Turbines and Power 134 - 011501 (2012).
- [34] N. Worth, J. Dawson, Combustion and Flame 160 (2013) 2476–2489.
- [35] U. Krueger, J. Hueren, S. Hoffmann, W. Krebs, P. Flohr, D. Bohn, in: ASME Turbo Expo, 2000-GT-0095, Munich, Germany.

- [36] W. Krebs, G. Walz, P. Flohr, S. Hoffmann, in: ASME Turbo Expo, 2001-GT-42.
- [37] L. Crocco, J. American Rocket Society 21 (1951) 163–178.
- [38] F. Nicoud, L. Benoit, C. Sensiau, T. Poinso, AIAA Journal 45 (2007) 426–441.
- [39] L. Benoit, F. Nicoud, Int. J. Numer. Meth. Fluids 47 (2005) 849–855.
- [40] A. D. Pierce, Acoustics: an introduction to its physical principles and applications, McGraw Hill, New York, 1981.
- [41] F. Silva, P. Guillemain, J. Kergomard, B. Mallaroni, A. Norris, Journal of Sound and Vibration 322 (2009) 255–263.
- [42] F. Nicoud, T. Poinso, Combust. Flame 142 (2005) 153–159.
- [43] R. Kaess, W. Polifke, T. Poinso, N. Noiray, D. Durox, T. Schuller, S. Candel, in: Proc. of the Summer Program , Center for Turbulence Research, NASA AMES, Stanford University, USA, pp. 289–302.
- [44] P. Wolf, G. Staffelbach, A. Roux, L. Gicquel, T. Poinso, V. Moureau, C. R. Acad. Sci. Mécanique 337 (2009) 385–394.
- [45] M. Heckl, M. Howe, Journal of Sound and Vibration 305 (2007) 672–688.
- [46] D. Zhao, Combustion and Flame 159 (2012) 2126–2137.